FACULDADE DE ENGENHARIA DA UNIVERSIDADE DO PORTO

Innovative Melt-Electrowritten Mesh Implants with Antistatic Properties for Pelvic Organ Prolapse Repair

Daniela da Silva Cruz

MASTER'S DISSERTATION

Biomedical Engineering Master's Degree

Supervisor: Dra. Maria Elisabete Teixeira da Silva

Co-Supervisor: Dr. Rúben Filipe Brás Pereira

24 June 2024

Innovative Melt-Electrowritten Mesh Implants with Antistatic Properties for Pelvic Organ Prolapse Repair

Daniela da Silva Cruz

Biomedical Engineering Master's Degree

24 June 2024

Abstract

Pelvic Organ Prolapse (POP) is a health condition that can significantly impact patients' quality of life. Most treatments available present drawbacks that can be solved with biodegradable implantable meshes, which can support the organs and replace the tissues as they regenerate. Moreover, the organism can completely absorb them without damaging the surrounding tissues.

3D Printing is a tool in the engineering arsenal that has beneficial applications in Tissue Engineering, for example, in producing scaffolds for POP repair. One promising technique for this application is Melt Electrospinning Writing since it allows a precise deposition of thin fibers, mimicking the fibrillar component of the native extracellular matrix. Incorporating antistatic agents in the polymer of interest is a way to stabilize the deposition and stretch these fibers even more, resulting in a reduction in their diameter.

The main goal of this dissertation was to study the influence of different concentrations (0.03, 0.06, and 0.1 wt%) of the antistatic agent Hostastat® FA 38 (HT) on the fiber's diameter and mechanical properties of Polycaprolactone (PCL) meshes. To do so, we blended the additive with the polymer and verified that with an increase in HT concentration, there was a reduction in the fiber's diameter of 14-17%, 39-45%, and 65-66%, depending on the mesh's geometry (square or sinusoidal). Both geometries included a pore size of 1.5 mm. These results proved that the antistatic agent could reduce the fiber diameter, as predicted, and the uniaxial tensile test results were in concordance with the expectations (higher diameter supports higher loads).

When comparing the PCL/HT curves with the pure PCL ones (with the condition of having similar diameters and the same geometry, in this case, square meshes), it was verified that PCL/HT meshes showed higher tensile strength and Young's Modulus values.

The cytotoxicity of these meshes was assessed through an Indirect Contact Assay, and the metabolic activity of the cells was measured using the resazurin assay. We also sterilized the samples via two methods: Ethanol + UV light and UV light only, having concluded that there was no statistically significant difference between these two methods. The cytotoxicity results were promising since no HT concentration provided cytotoxic effects on the PCL/HT meshes.

Incorporating this antistatic agent revealed promising results, making it possible to obtain stable and thinner filaments that present higher tensile strength and Young's Modulus values compared to PCL meshes. By adding no toxicity to the cells, a further study on the interaction between the polymer and the additive would be of great interest to understand how the meshes' mechanical performance is being enhanced.

Developing a mesh that is thinner, more stable, and still mimics the vaginal tissue's mechanical behavior (by supporting similar values of stress and presenting a similar level of stiffness) could be an innovative solution for POP repair.

Resumo

O Prolapso de Órgãos Pélvicos (POP) é uma condição de saúde que afeta significativamente a qualidade de vida dos pacientes. A maioria dos tratamentos disponíveis apresentam algumas desvantagens que podem ser resolvidas com malhas implantáveis biodegradáveis, que suportam os órgãos e substituem os tecidos enquanto os mesmos regeneram. O organismo irá absorver completamente as malhas sem danificarem os tecidos vizinhos.

A Impressão 3D é uma ferramenta muito útil na área da engenharia especialmente na área da Engenharia de Tecidos, por exemplo na produção de scaffolds para a reparação do POP. Uma das técnicas de Impressão 3D mais promisoras para esta aplicação é o Melt Electrospinning Writing, uma vez que permite imprimir filamentos mais finos, de forma mais estável e, assim, replicar microestruturas de interesse. Uma das formas de estabilizar e reduzir ainda mais o diâmetro das fibras é a incorporação de agentes antiestáticos no polímero pretendido.

O principal objetivo desta dissertação era estudar a influência de diferentes concentrações do agente antiestático Hostastat® FA 38 (HT) no diâmetro da fibra de malhas de Policaprolactona (PCL) (0.03, 0.06, and 0.1 wt%). Para isso, misturou-se o aditivo com o polímero e verificou-se uma redução no diâmetro da fibra de 14-17%, 39-45%, e 65-66%, respetivamente, dependendo da geometria da malha (quadrada ou sinusoidal). Ambas as geometrias apresentavam um poro de 1.5 mm. Os resultados corroboraram o que era esperado (a redução no diâmetro), e os resultados dos testes de tração uniaxiais também se revelaram de acordo com as expectativas (quanto maior o diâmetro, maior o valor do *stress* que a malha suporta).

Para comparar as curvas das malhas PCL/HT com malhas de PCL puro, foram escolhidas malhas com diâmetros semelhantes e a mesma geometria, que neste caso foi quadrada. Verificou-se que as malhas PCL/HT apresentam maiores valores de *tensile strength* e módulo de Young.

Para testar a citotoxicidade das malhas, fizemos um Ensaio de Contacto Indireto e a atividade metabólica das células foi medida através de um ensaio de resazurina. A esterilização das malhas foi feita através de dois métodos: Etanol + luz UV e apenas UV, sendo que não houve diferenças estatisticamente significativas entre estes métodos nos resultados. Os resultados de citotoxicidade foram bastante promissores sendo que nenhuma concentração de HT provocou efeitos citotóxicos nas malhas.

A incorporação deste aditivo revelou resultados promissores, sendo possível obter filamentos mais finos, mais estáveis, e com maiores valores de *tensile strength* e módulo de Young, do que os obtidos com o polímero puro. Ao não causar nenhuma toxicidade às células, é de maior interesse prosseguir com o estudo da interação entre o aditivo e o polímero e perceber como é que a *performance* mecânica destas malhas poderia ser melhorada.

Ao desenvolver uma malha mais fina, estável e que ainda assim, mimetiza o comportamento mecânico do tecido vaginal (ao suportar valores semelhantes de carga e níveis de rigidez idênticos) poderíamos desenvolver uma solução inovadora para o reparo do POP.

Acknowledgments

First and foremost, I would like to extend my sincere thanks to my supervisor Dra. Maria Elisabete Teixeira da Silva and co-supervisor Dr. Rúben Filipe Brás Pereira for the guidance and motivation provided throughout the development of this dissertation.

I would also like to express my gratitude to my colleagues at Laboratório de Desenvolvimento de Produto e Serviços for the support and motivation provided when I needed it most. I also want to thank Luís Bebiano for all the guidance in cell culture assays and support in a subject I was not comfortable with.

I must also express my gratitude to my family, boyfriend, and friends for their support throughout my academic journey, for offering assistance during challenging times, and for turning my last five years into memorable and joyous experiences.

Lastly, I gratefully acknowledge the Emprego Científico 2021.00077.CEECIND and the project PRECOGFIL-PTDC/EMD-EMD/2229/2020, Funded by FCT. This work was supported by FCT, through INEGI, in the scope of LAETA, project UIDB/50022/2020 and UIDP/50022/2020.

Daniela da Silva Cruz

Contents

List of Figures

List of Tables

Chapter 1

Introduction

1.1 Motivation

Pelvic Organ Prolapse (POP) is a medical condition that significantly impacts the patient's quality of life, and it's particularly prevalent among women between 40 and 60 years old [1]. This condition affects 41% of women over 60 [2], with a lifetime prevalence of 30% - 50%. In 11% - 12% of the cases, a woman with an average life expectancy must have a surgical intervention for prolapse or incontinence, with a re-operation rate of 29%, by the age of 79 [3]. It is estimated that 10 - 15% of women in developed countries will have surgery for POP repair during their lifetime [4].

Initially, in the 1970s, gynecologists used free-form grafts for pelvic floor reconstructive surgery, although it was necessary to cut them into different shapes, which was unsafe. Then, medical device manufacturing companies started to develop mesh-based kits in various shapes and sizes. In 2002, the Food and Drug Administration (FDA) approved the first prosthesis for POP treatment. Since then, the research on these meshes has grown to the point that synthetic surgical meshes were developed as an alternative to biological grafts [5]. The main goal of using these meshes was to reinforce the pelvic organ tissues and prevent the recurrence of symptoms [4].

Most of these meshes were based on Polypropylene (PP) [2, 5], an inert and biocompatible material with good fatigue, durability, and sustainable tensile strength [2]. The Therapeutic Goods Administration showed that between 2005 and 2013, 3.7 million synthetic meshes were implanted worldwide [4]. However, the insertion of these meshes has been associated with graft-related complications [2], such as erosion into the vagina, infection, pain, and discomfort [4]. This was due to their tendency to adhere to the viscera and induce a high inflammatory response. Its stiffness also increases over time, causing the weakening of the surrounding tissues [5].

Due to all these problems, the FDA has banned synthetic meshes for transvaginal prolapse repair, which led to the development of novel tools, including novel materials, for POP repair [2]. The ideal material should be sterile, low-cost, non-carcinogenic, durable, and have minimal risk of infection. Also, these meshes should be able to support the weight of the pelvic tissues and be resistant to compression [5].

A possible solution to this problem is using non-textile biodegradable implants, which can be produced by Melt Electrospinning Writing (MEW). MEW is a 3D Printing technique that allows the deposition of nano- to micro-meter filaments layer-by-layer to create scaffolds, which can be a powerful tool for Tissue Engineering applications [2, 6]. Printing structural features on a micrometer or nanometer scale are necessary for biomedical applications, as this approach aims to replicate the tissue's microarchitecture, which can be achieved with MEW [7]. However, printing thin and stable fibers is not always possible, and it can be achieved by blending the desired polymer with an antistatic agent [8].

1.2 Objectives

The main goal of the dissertation is to evaluate the influence of different concentrations of an antistatic agent on the fiber diameter and mechanical properties of biodegradable meshes made of Polycaprolactone (PCL). This will be accomplished by mixing PCL with an antistatic agent, Hostastat® FA 38 (HT), to mitigate the impact of electrostatic forces during the printing process. Additionally, the influence of the predefined geometry of the fibers will be studied.

The specific objectives of this thesis are:

1. Incorporating HT in medical-grade PCL meshes (with different geometries).
2. Evaluate the effects of using an antistatic agent on the mechanical properties of the biodegradable meshes through different weight percentage (wt%) values of HT.
3. Perform mechanical tests (uniaxial tensile tests) on the meshes and compare the performance of the different meshes.
4. Evaluate the cytotoxicity of the meshes, depending on the wt% value of HT used.

1.3 Dissertation Structure

This dissertation is structured as follows:

- Chapter 2: Describes the anatomy of the female pelvis and the pelvic floor dysfunction, namely POP. It also describes the treatments available for this condition and future treatment perspectives.
- Chapter 3: Describes the Additive Manufacturing background, explaining the subtypes of Electrospinning techniques, highlighting MEW and its applications and advantages. The effects of the electrical field on the jet are also explored in detail. In this chapter, the definition of antistatic agents will also be given, as well as the effects these agents can have on the melt-electrospun fibers.

- Chapter 4: In this chapter, an outline of the methodology is explained, detailing the MEW prototype, materials used, and protocols necessary to accomplish all the predefined objectives for this dissertation.
- Chapter 5: In this chapter, the process of the MEW device calibration was described in detail, showing all the printing parameters used and the effect they had on the filament. This calibration was performed for both technical and medical-grade PCL.
- Chapter 6: In this chapter, we present the PCL/HT filaments' diameters' measurements and the results of the uniaxial tensile tests and cytotoxicity evaluation. In this chapter, we also discuss the relevant results.
- Chapter 7: This chapter presents the main findings and suggestions for future work.

Chapter 2

Female Pelvis Anatomy and Pelvic Floor Dysfunctions

In this chapter, a brief introduction about the female pelvic area will be given, which consists of the pelvic floor and vaginal tissue. Treatments available for pelvic floor dysfunction, namely POP, will also be introduced in the following chapter.

2.1 Anatomy of the Female Pelvis

To comprehend how pelvic floor dysfunction can affect the quality of life of a patient, it's necessary first to understand the complex structures of the pelvic anatomy.

The pelvis occupies the middle part of the human body, separating the lumbar region of the abdomen and the inferior members [9]. The pelvis plays different vital roles, such as providing structural support and stability to every movement, like walking or even standing, and by supporting all the abdominal organs and, in the case of the woman, supporting childbirth [9, 10].

Men's pelvis is heavier and thicker than women's pelvis. A male's pelvis has a heart-shaped inlet, while the female pelvis is usually more circular and larger, which can lead to pelvic floor weakness. Figure 2.1 shows the structure of both male and female pelvis, in which can be seen that the pubic arch is larger in women (80º - 85º) when compared with men (50º - 60º) [11].

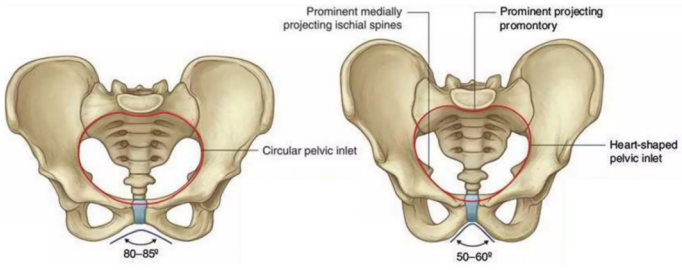

Figure 2.1: Structure of bone pelvis in women (left) and men (right) [11].

The pelvis region covers the bony pelvis, the pelvic floor, the pelvis cavity, and the perineum [9]. The bony pelvis, or pelvic bones, is composed of the sacrum, ilium, pubis, and ischium, and it's divided into two different regions by the pelvic brim. The false (greater) pelvis - the abdominal cavity that contains the superior region - and the true (lesser) pelvis - the pelvic cavity that includes the inferior region and is closed by the pelvic floor [11, 12]. The pelvic bones' primary functions are supporting the weight of the structures above and protecting the pelvic and abdominopelvic viscera [9]. Figure 2.2 shows the anterior view of the pelvic bones.

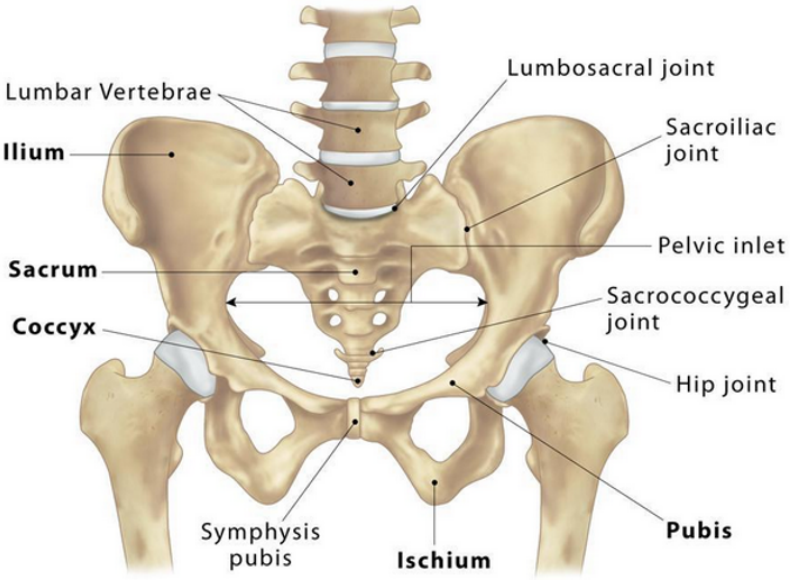

Figure 2.2: Anterior view of the pelvic bones, adapted from [13].

The pelvic girdle consists of the anterior part of the bony pelvis, which is composed of the pubis, ischium, and ilium, and it's connected posteriorly to the pelvic spine (coccyx and sacrum). The innominate bones are set of the pubic, ischial, and iliac bones, so each individual has two innominate bones (one at each side) [9].

The pelvic cavity consists of the space between the pelvic bones and is limited by the abdominal cavity superiorly, the pelvic floor inferiorly, and the sacrum and coccyx posteriorly. Inside this cavity are the urinary bladder, pelvic colon (sigmoid colon), rectum, reproductive organs, and other structures and tissues [9].

The pelvic floor (as shown in Figure 2.3) is a muscular layer that separates the pelvic cavity from the perineum (which lies inferiorly to the pelvic floor), supporting the weight of the viscera (urinary bladder, pelvic colon, rectum, anus, uterus, and vagina in females) [9]. Being a muscular layer, the fibers of the pelvic floor will provide active support through contraction and relaxation of the muscles [14]. For instance, these muscles will have a sphincter action on the rectum and urethra (preventing incontinence) [9].

The perineum is a diamond-shaped area between the pubic symphysis and the coccyx [9]. It comprises the posterior anal triangle and the anterior urogenital triangle, which corresponds to the external genitalia, the vulva [1].

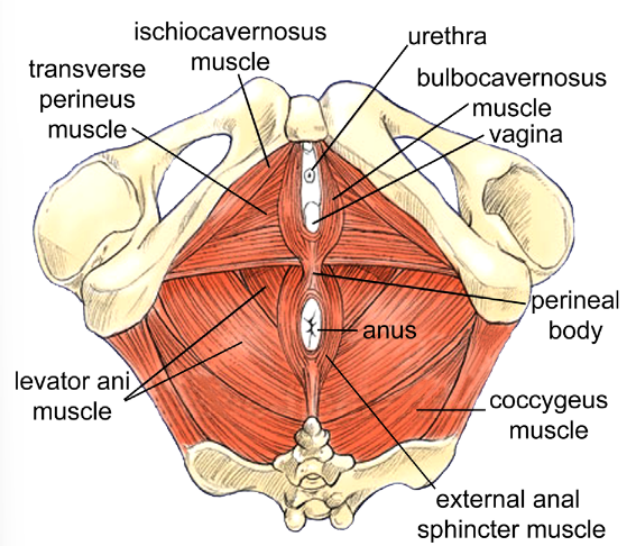

Figure 2.3: Scheme of the anatomy of the female pelvic floor muscles [15].

2.2 Pelvic Floor Dysfunctions: Pelvic Organ Prolapse

The pelvis is a complex structure that is understudied biomechanically. The pelvic structures must manage the changes in the abdominal pressure (that comes with the patient's daily activities) and prevent incontinence and POP. At the same time, it has to allow urination and defecation, and also childbirth, in the case of women [16].

Pelvic Floor Dysfunctions include different disorders, such as urinary and anal incontinence, sexual disorders, and POP (the focus of this dissertation). This type of disorder has a significant impact on both the physical and psychological state of women [17].

POP consists of the prolapse of one or more pelvic organs (uterus, vagina, bladder, bowel) through the vagina due to the weakness of the pelvic floor support tissues [18, 19]. These support tissues are mainly fascia and ligaments, and their function depends on the connective tissue's extracellular matrix (ECM). The main components of the ECM are collagen, elastin, proteoglycans, and glycoproteins, being collagen responsible for supportive function [20].

Studies have shown that collagen types I and III are present in the female pelvic floor structures. Collagen I affects tissue stiffness, and Collagen III affects tissue elasticity, so naturally, reductions in collagen levels can lead to poor pelvic floor support. It was also shown that women that suffer from POP have a decrease in vaginal wall thickness, which can be caused by a reduction in collagen, elastin, and smooth muscle levels [20].

Some of these supporting tissues are the *levator ani* and *coccygeus* muscles (Figure 2.3), and it has been reported that women with POP present a reduction in the thickness of the *levator ani* muscle. The perineal body (Figure 2.3) is another essential structure that can lead to POP when its strength is reduced [15].

The different types of prolapse are listed below, and some are represented in Figure 2.4.

- Upper vaginal prolapse

  - Uterus
  - Vaginal vault: after hysterectomy, when the top of the vagina falls
- Anterior vaginal wall prolapse
  - Cystocele: bladder descends
  - Urethrocele: urethra descends
  - Paravaginal defect: pelvic fascia defect
- Posterior vaginal wall prolapse
  - Enterocele: small bowel descends
  - Rectocele: rectum descends
  - Perineal deficiency

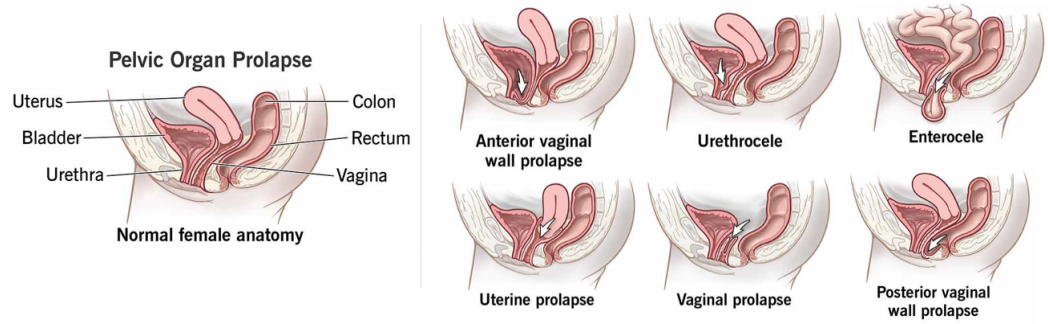

Figure 2.4: Representation of different types of POP, adapted from [21].

Almost 50% of women above 50 (that already had one or more vaginal childbirth) will suffer from POP [22]. It's also estimated that 45% of the female population will be affected by POP due to the aging of the population [15].

POP is strongly associated with pregnancy, childbirth, menopause, and aging [19, 23]. This disease also has a genetic predisposition, meaning that people with a history of POP in the family are more likely to develop this condition [20]. Considering the aging of the population, it's expected that the number of POP occurrences will increase in the future [17, 18]. Physical stress [24] and intra-abdominal pressure (like chronic pulmonary disease, constipation, and obesity) [3] are also risks that can lead to POP.

Not all women suffer from a specific symptom, but most of the time, women experience discomfort in the vagina and bladder, bowel, and/or sexual dysfunction [18, 19, 23, 24]. Some other symptoms include pelvic heaviness, bulge or protrusion coming down from the vagina, and backache [19]. Beyond physical pain/changes, this condition will undoubtedly affect women's quality of life with psychological and sexual impacts [18], so there's a need to manage POP and develop new treatments to improve the quality of life of the patient.

2.3 Treatments for Pelvic Organ Prolapse

Treatments for POP include nonsurgical (conservative management and use of mechanical devices) and surgical options (invasive) [3]. The decision about the type of treatment is based on the degree of the prolapse, the surgeon's experience and capabilities, the symptoms, and the well-being of the woman [19].

2.3.1 Nonsurgical treatments

Conservative treatments are used when the prolapse is not in an advanced stage, when the woman still wants to have children, and when the patient declines surgery [19]. This type of treatment includes behavioral modification (like weight loss and avoiding heavy lifting [18]) and pelvic floor muscle exercises. These treatments will lead to a reduction of symptoms, an increase in the strength of the pelvic floor musculature, and the prevention of worsening the condition and delaying surgery [3].

Nonsurgical treatments also include the use of pessaries, which consist of removable devices that provide support after prolapse [18] (Figure 2.5). Most pessaries are made of medical-grade silicone [3] and are used as the first-line treatment if surgery is not possible or not accepted by the patient [18]. This device also presents contraindications like the vagina being too short or the patient being unable to manage the device on her own since it will be inserted and removed periodically [3].

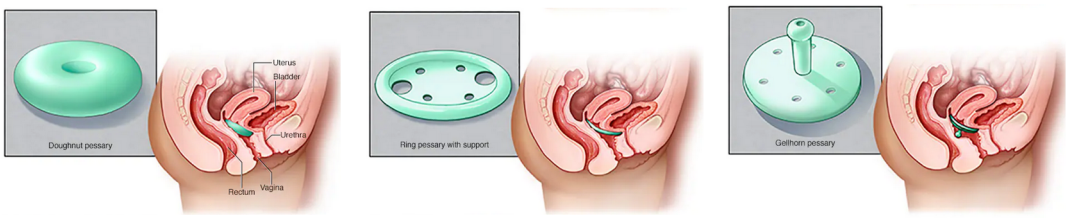

Figure 2.5: Different types of pessaries that can be used for POP treatments, adapted from [1].

2.3.2 Surgical treatments

It is estimated that 6 - 18% of POP patients undergo surgical treatments [20] that, unlike conservative treatments, aim to correct anatomic defects, which can be done through different approaches [3]. The selection of the type of intervention will depend on the severity of the POP, the type of symptoms that affect the patient, and the surgeon's ability and decision, among other factors [18]. Below is a list of different approaches used.

- Restorative surgery - use of the patient's endogenous supportive tissue
- Compensatory surgery - use of synthetic meshes or biological grafts
- Obliterative surgery - closes partially or totally the vagina

POP is one of the most important clinical problems that influence the quality of life of women [22] and is the main reason that women undergo gynecological surgery [25]. In most cases, conservative methods are not enough, so there's a need for an invasive treatment associated with low rates of recurrence and complications, especially when considering the aging of the population [24]. Throughout a woman's life, there's a chance of 12.6 - 20% [23–25] of having prolapse surgery, being the incidence of POP surgery highest among women aged 60 to 69 years [26]. Unfortunately, in 3 - 6% of the cases, the woman will still feel symptoms after surgery [25].

Synthetic meshes

Since the mid-1990s, compensatory surgeries using synthetic polymeric meshes for POP have been adopted [18] as an additional reinforcement for treating POP. It has been shown that using these meshes provides a relatively low recurrence rate compared to traditional fascial repair surgery [22]. These permanent meshes aimed to support the prolapsed organs while the damaged tissues were restored and the pelvic muscles gained strength without harming the surrounding tissues [15].

Most meshes available on the market are knitted and manufactured from different polymers. The most common one is Polypropylene (PP) [27], an inert and biocompatible material (Figure 2.6). PP-meshes are durable, favor tissue growth, and have mild inflammatory responses. However, they adhere to the viscera [15]. Restorelle® mesh, made by Coloplast [28], is one of the latest clinical implants for POP repair [27]. It's a lightweight (density of 19 g/m^2) PP-mesh that can be used in anterior or posterior vaginal prolapse [26].

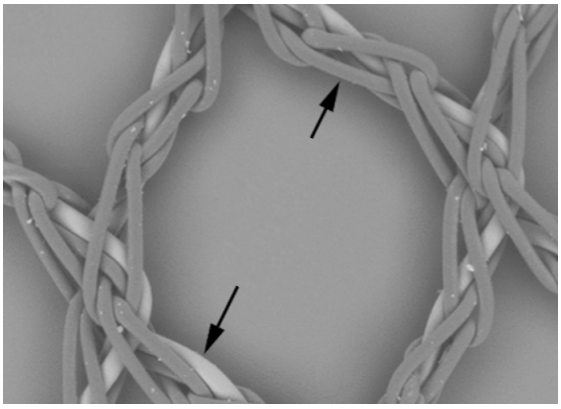

Figure 2.6: Scanning electron microscopic (SEM) image of a PP-mesh. Adapted from [29].

Besides all the benefits of using synthetic meshes in this type of intervention compared to traditional surgery (where native tissue is used), the safety of meshes was a concern for an extended period. In 2008, the United States FDA denoted the high rate of serious complications associated with synthetic meshes. Mesh protrusion into the vaginal wall, infection, dyspareunia, inflammation, and erosion of the surrounding tissues were some of the downsides of using synthetic meshes. In 2011, the FDA pointed out that these complications were not casual and that the leading causes could be mesh material, size, and shape. As a result, many meshes were removed from the market,

and the use of synthetic meshes in pelvic surgery was reduced [15, 18, 24, 25]. In 2019, the FDA prohibited all manufacturers from selling and distributing synthetic meshes for transvaginal repair of POP in the United States [30].

The mesh-related complications observed were influenced not only by the chemical properties of the material but also by its design and mechanical properties. PP-meshes become stiffer with time, which may be caused by changes in the biomechanical properties once the mesh is integrated and reacts with the tissue. The pore size is another crucial aspect of the biomechanical response of a mesh. Large pore sizes induce cells to produce collagen within the mesh filaments, increasing the mesh stiffness and causing pain to the patient [29].

Together with many other synthetic meshes, Restorelle® was also removed from the market by the FDA due to a lack of "confidence in the safety and effectiveness of these devices" [27]. Rynkevic et al. [27] performed uniaxial tensile tests on both Restorelle® mesh and vaginal tissue to compare their mechanical behavior (Figure 2.7). The authors concluded that the synthetic mesh is stiffer than the vaginal tissue, which will lead to damage to the surrounding tissues and possibly inflammation and infections.

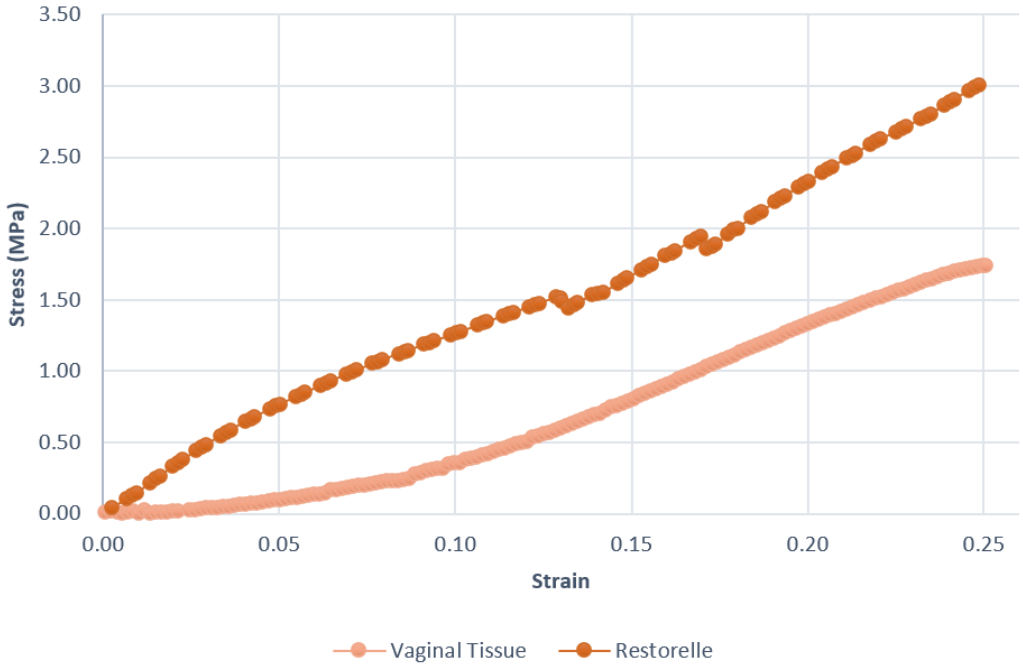

Figure 2.7: Mechanical behavior of Restorelle® mesh and vaginal tissue, when performing a uniaxial tensile test. Adapted from [27].

Biodegradable meshes: future solution

Due to the high risks associated with synthetic meshes, a recent focus has been on designing biodegradable surgical meshes. The primary objective is to enhance the device's biocompatibility and reduce the inflammatory response. However, identifying the ideal characteristics that a mesh

should possess remains unspecified, making this task more challenging. Biochemically, these meshes should be non-carcinogenic, inert, and resistant to sterilization and infections. Mechanically, it should be able to support all the mechanical actions and mimic the tissue behavior in loading situations [15].

The intended application of these meshes is POP repair. Thus, attempting to replicate the characteristics of existing synthetic meshes on the market is beneficial. If we can demonstrate that biodegradable meshes perform comparably to synthetic ones while addressing their drawbacks, we may offer a better solution for POP repair.

It is believed that **mesh porosity** affects its biocompatibility and host tissue ingrowth [15, 27, 31]. However, there is no agreement on the ideal pore size. Larger pores (> 1 mm) are proven to exhibit less inflammatory responses, calcification, and fistula formation (an abnormal connection between two structures) than meshes with small pores [32], while avoiding pore collapse [27]. In their study, Knight et al. [31] concluded that if pore size < 1 mm, there's a higher chance of inflammation and development of connective tissue, which can cause pain to the patient. They also state that this pore size is critical for tissue ingrowth, leading to encapsulation of the mesh, which causes pain [31].

For instance, Restorelle®, which is no longer available commercially, was available with different diameters and pore sizes. Buying them with diameters of 80, 160, and 240 μm and pore sizes between 1.6 - 2 mm [27] was possible. A large pore size like 1.6 - 2 mm also favors tissue ingrowth [27], establishing a 1 - 2 mm range for adequate pore size. With this in mind, choosing a pore size of 1.5 mm seems to be appropriate to proceed with this study.

The **mesh stiffness** is one of the most critical parameters to have in mind. Stiffness is a mesh characteristic defined by the slope between the tension applied to the mesh and the strain it will suffer. The problem with this characteristic is that if the stiffness is too low, the mesh cannot support the weight of all the structures above. If it is too high, it will lead to erosion and damage to the surrounding tissues. This can be explained by introducing the concept of "stress shielding", which states that if a structure that usually supports a lot of weight suddenly stops loading a big part of it (which the mesh will support), it will degenerate due to a decrease in the level of strain to which it is used to be submitted [15].

The **mesh geometry** can also greatly influence its behavior when under tension. In that way, during the dissertation, it was chosen to print squared meshes (mimicking Restorelle®) and sinusoidal ones. Sinusoidal meshes are believed to mimic the collagen and ligament geometries better and behave similarly to the soft tissues under tension [33].

Chapter 3

Additive Manufacturing Background

Additive Manufacturing will be introduced in this chapter, as well as the Electrospinning technique, so the reader can understand the basic concepts of 3D printing. After that, a brief overview of MEW will be given since it is the technique used during the dissertation. At the end of the chapter, the definition of antistatic agents will be provided, as well as the motivation to use this type of additive in MEW-printed meshes.

3.1 Additive Manufacturing

In the last few years, Additive Manufacturing (AM) has revealed new product production methods. AM, or 3D Printing, is based on the principle of fabricating an object by adding successive layers of material under computer control [34]. This approach allows the manufacturer to have more control over the final product's design [6], even on the small details.

A wide range of materials can be used with this technique [35], being the main categories plastics, metals, ceramics, and composites. The different techniques available can also be categorized by the raw material used [34], as listed below.

- **Powder-Based:** Selective Laser Melting (SLM); Selective Laser Sintering (SLS); Electron Beam Melting (EBM)
- **Liquid-Based:** Stereolithography Apparatus (SLA); Polyjet
- **Solid-Based:** Laminated Object Manufacturing (LOM); Fused Deposition Modeling (FDM)

AM Strengths and Limitations

Besides the possibility of using different materials, this technique also offers other advantages compared to conventional methods. This low-cost technique [35] is targeted to small-scale production so every product can be customized easily, unlike conventional techniques that are inclined to mass-production [34].

Conventional processes involve operational, assembly, and inspection phases, which require a certain level of expertise to handle. AM solves that problem since it's possible to print the objects together simultaneously, discarding the assembly stage (reduced costs). Additionally, AM also drastically reduces material waste and production time. Another advantage this technique provides is the ability to create complex designs [34].

As with every other printing method, this also presents its drawbacks. The surface quality of AM products is worse than the ones obtained with conventional manufacturing techniques. In AM methods, the material cools down quickly, forming distortions that can impact the material's behavior under stress [36]. While still comparing AM to conventional techniques, AM presents many limitations in producing large one-piece structures (because it depends on the printer's dimensions) and is unsuitable for mass production [37].

Furthermore, it is possible to use any material in an AM method (polymer, ceramics, metals, and composites) in any state (powder, liquid, solid). However, depending on the product's final application, finding an adequate processing material may be difficult, which leads to post-treatments to improve the material's surface properties [36, 37].

AM Applications

When designing a product, it is necessary to consider its intended use and its material/composition. Different AM techniques can be used for the same application, so the process must start with the requirements of printing the desired product and then choose the adequate technique [34].

AM techniques can be used in several areas, such as automotive, aerospace, medical, and casting industries [34]. AM models can also be used for educational purposes and preoperative planning of complex surgeries [38]. Moreover, since it is a computer-aided technique, it is possible to use information from imaging techniques to customize the implant or device of a patient [6, 38].

Exploring the medical field, AM has gained traction in the Tissue Engineering field [39]. When designing a device or implant replicating the tissue architecture, it's essential to print all the structural features on a micro or nanometer scale [7]. AM allows printing scaffolds with the desired porosity, shape, and geometry [39], ensuring that cell adhesion and growth are viable [35].

3.2 Electrospinning

Electrospinning is an AM method, introduced in 2001 [40], based on applying a high voltage to a melt polymer or to a solution that forms a charged jet and is drawn to a collector [41–44]. This technique allows the production of nanofibrous architectures, which is very appealing to the Tissue Engineering field [40].

Electrospinning relies on the mobility of ions, meaning that the movement of ions when the electric field is applied will cause surface changes [45]. The material will be pushed towards the collector by electrostatic forces between the electrical charges carried by the polymer jet and the applied electrical field [42].

The standard setup of an electrospinning device comprises a pump, a syringe, a nozzle, a high-voltage power supply, and a collector plate [41]. However, there are several ways to heat a polymer or deliver it to the nozzle [40], so it's possible to have different configurations for this device. The main ones are a spinneret, an electrical power supply, and a collector, placed in this specific order [42]. Figure 3.1 presents a scheme illustrating the working principle of electrospinning.

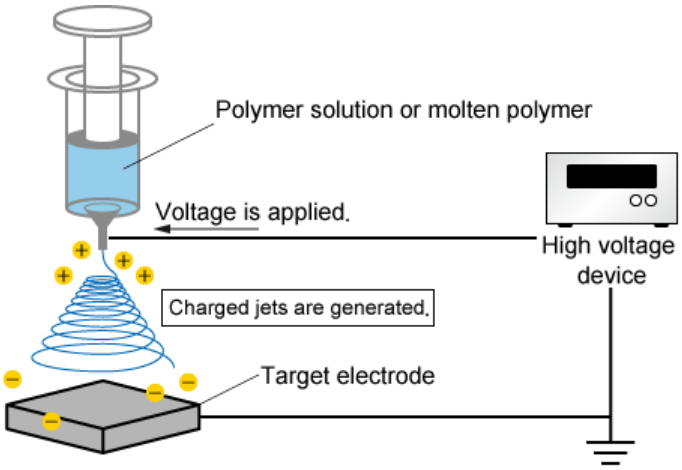

Figure 3.1: Representation of the main components of an electrospinning device [46].

The polymer is supplied from the spinneret attached to a feeding system. Depending on the method used, this system can either be a syringe (air pressure) or an extruder (including adjustable heating elements to melt the polymers), which allows the use of single or multiple needles or nozzles to extract the material [42].

3.2.1 Electrospinning techniques

Electrospinning comprises the methods of Solution Electrospinning (SES) and Melt Electrospinning (MES). In SES, the polymer is dissolved in a solvent, forming a solution, while in MES, the polymer is melted without adding any solvent to it [41].

SES is the most widely used for producing submicron fibers. However, the solvent can be very expensive, and the implant's cytotoxicity could be an issue, not making it suitable for biomedical applications [41]. Moreover, producing a solution electrospun mesh will require inducing porosity since this method will deposit the fibers without much precision. This could lead to a mesh without sufficient pore size for cell adhesion [40].

The potential cytotoxicity of solvents can be solved using MES since it is a solvent-free technique, making it suitable for producing cell scaffolds. Fibers with diameters ranging from micro to nanoscale can be created with this technique [41]. Moreover, the polymer melt presents higher viscosity when compared to the SES technique, which will provide a more stable deposition and higher precision. MEW consists of the same method as MES with an integration of a computer-controlled head that will allow the deposition of highly ordered fibers (direct writing) [35]. This technique will be later explored in Section 3.3.

3.2.2 Materials used in Electrospinning

Electrospinning allows one to create nanofibers using several types of materials, such as organic polymers, small molecules that can self-assemble and make a sufficient chain entanglement or colloidal particles [47].

Polymers, ceramics, and composites can produce fibers through Electrospinning as long as they can be melted or used as a solution. Polymers are the most common material used in electrospinning, providing easy-to-produce fibers compared to other materials [42]. PCL is a polymer commonly used to produce electrospun fibers for biomedical applications. This polymer will be used during this dissertation and explored later in Section 4.2.1.

3.2.3 Advantages of Electrospinning

Electrospinning is a low-cost and straightforward method that allows researchers to develop different products using several polymers compatible with this technique [40]. This technique has gained traction among researchers since it's cost-effective, easy to handle, and versatile for fiber production [40, 42].

Electrospinning is appealing compared to other techniques, like wet spinning or extrusion molding methods, because it only takes a few steps to obtain the product [42]. Besides that, it allows us to blend different polymers and inject that mixture into the feeding system to get fiber with more desirable mechanical properties. Another advantage is the possibility of using any substrate as a collector plate, including metal, nonwoven mats, and commercial membranes [48].

3.3 Melt Electrospinning Writing

Melt Electrospinning Writing (MEW), or Melt Electrowriting, is a high-resolution AM method [7] that combines some principles of Electrospinning and Melt Extrusion techniques [6], resulting in fiber diameters in the range of $5 - 30\ \mu m$ [49].

Every MEW device must include a printing head, nozzle, heating system, delivery system, high voltage power supplier, moving collector, and a computer [48, 50]. The printing head will store and heat the polymer until it melts and is supplied to the nozzle. Between the nozzle and the moving collector, there is an electric field that will draw the polymer into the collector, as seen in Figure 3.2 A. Due to the electric field, the material will be under the influence of electrostatic forces that form the Taylor's cone (later explored in subsection 3.3.1) at the end of the nozzle [6, 48, 50], and then make the material flow steady while regulating the fiber jet's diameter [6, 7]. The MEW process can be seen in Figure 3.2 B.

As requirements for a functional MEW device, every device must have a supply zone where the molten polymer can be delivered to the spinneret; there must be a fiber collection zone; the polymer should be sufficiently charged to form the Taylor's cone that is drawn as a polymer jet on the collector (where the polymer will then cool down and solidify) [51].

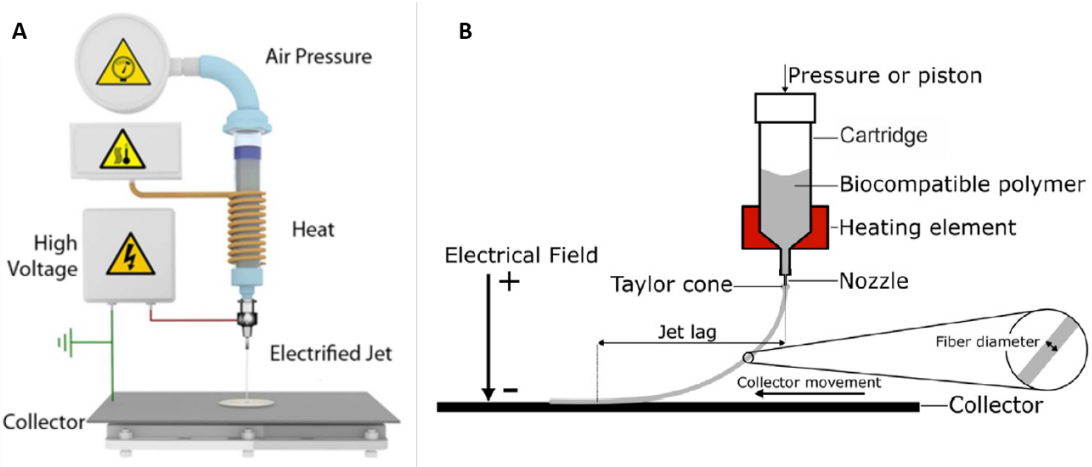

Figure 3.2: Main components of a MEW device, adapted from [38] (A), and representation of MEW process (B).

3.3.1 Effect of the electrical field on the jet

It is easy to understand that when printing a scaffold or a model, it is desired to obtain the same fiber diameter as planned to avoid defects and ensure good structural strength [52]. It is then essential to understand how the jet behaves under the effects of the electrical field and how it will influence the fiber diameter.

When the polymer is in the nozzle, it will be charged by the electric field, making it exit the nozzle and form a droplet. This droplet will then be distorted, forming the Taylor's cone, and at the apex, a jet of fluid starts to form [48, 51]. Figure 3.3 shows the interaction of forces involved in the cone formation.

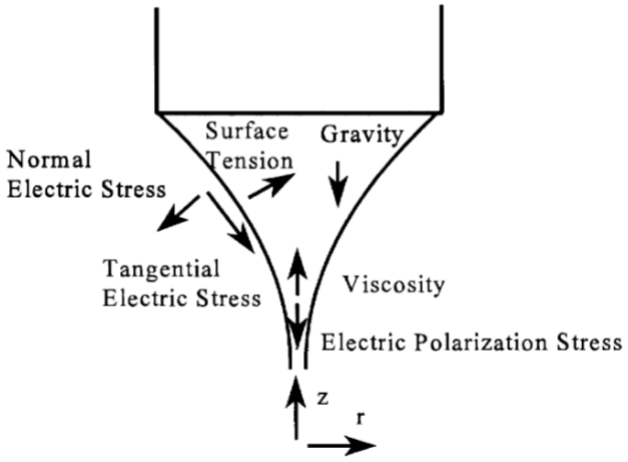

Figure 3.3: Forces present in the Taylor's Cone formation [50].

Electrostatic forces will then pull the charged jet to the oppositely charged collector, stretching the jet and decreasing the fiber diameter. Besides, these forces will also improve the stability of

the jet, leading to a more controlled process [50, 52].

Viscosity is one of the forces involved in this process, and its relation to electrostatic forces will dictate the fiber's diameter. A perfect balance between viscosity and electrostatic forces will lead to thinner and more controlled fibers. However, if these forces cannot counteract the viscosity, the jet will not be stretched enough, and the filament will be thicker. In the opposite scenario, the jet will not be stable, and the fiber will be irregular [50].

3.3.1.1 Influence of printing parameters on the fiber characteristics

As shown, both electrostatic forces and viscosity present will influence the stability and diameter of the jet. The viscosity is highly influenced by some printing parameters such as the temperature, voltage, distance between the nozzle and collector, and the collector's speed [52], so it is crucial to understand how they can influence it.

In this subsection, there will be a discussion about the influence of these parameters on the fiber diameter. It is to be noted that these should be defined before printing and must remain constant while printing [33].

Temperature

The temperature will define (approximately) the temperature at which the polymer leaves the nozzle. Specifically for PCL, rheological studies showed a decrease in viscosity with an increase in the temperature [33]. The viscosity is still high when the temperature increases, so the jet becomes thicker. As the temperature rises, the viscosity will decrease to the point that the jet is stretched and thinner fibers are obtained [50].

Xie et al. [52] confirmed this point by studying the effect of printing parameters on the size of PCL fibers printed by MEW and concluded that when the temperature is set too high, the viscosity is too low, leading to a high melt fluidity and a thinner jet [52].

Voltage

The voltage applied between the nozzle and the collector will create an electric field that charges the polymer flow and pulls it toward the collector. If the voltage is set too low, it is possible that the polymer is not attracted to the collector as it should. The distance between the nozzle and collector will also influence the value of voltage needed to extrude the polymer properly [33].

The fiber diameter will also limit the voltage needed. A small fiber diameter at high voltage produces a spinning effect on the polymer jet (it will not be defined as desired) [33]. Xie et al. [52] studied the influence of voltage on the fiber diameter and concluded that if we increase the voltage applied, the fiber diameter will decrease.

Distance between Nozzle and Collector

As mentioned before, the distance and the voltage must be matched when defined since they are dependent on each other. Studies [33] showed that if the distance is too high, there's a loss in the geometry accuracy and print quality. If the distance is too low, the jet cannot be properly formed, affecting the print quality.

Xie et al. [52] also studied the influence of the distance between the nozzle and the collector on the fiber diameter and concluded that an increase in the distance leads to a decrease in the diameter.

Collector's Speed

This parameter will directly affect the reproduction of the programmed geometries. The jet will not be deposited on the right coordinate if the collector's speed is too high, leading to an inaccurate geometry [33].

He et al. [53] studied the influence of several printing parameters on the fiber diameter and concluded that collector speed is one of the parameters with a bigger impact on it. Xie et al. [52] figured that an increase in the speed of the moving collector leads to a continuous decrease in the fiber diameter.

3.3.2 Advantages of Melt Electrospinning Writing

Even though less than 1% of the literature on Electrospinning techniques focuses on MEW [51], there are still many advantages to using this technique.

MEW devices are easily customizable, making it possible for every research group to build their own device to correspond to their necessities. This option is still cheaper than one standard filament fabrication equipment [51].

MEW provides a continuous and fluid polymer jet due to the application of a high voltage between the nozzle and the moving collector [54]. The melt jet is stable, which leads to a more predictable fiber deposition [51], enabling the production of ordered structures like scaffolds with well-defined pore size and geometry [50]. It also allows obtaining fibers thinner than those obtained through SES [54]. The moving collectors increase the deposition's accuracy and allow the fabrication of layer-by-layer structures with specific designs and shapes [55]. Comparing MEW to SES, MEW provides more control of the fiber deposition, and consequently, the structures would be more similar to the designed ones (shape, volume, architecture) [51]. The schematic representation presented in Figure 3.4 illustrates these differences between the two techniques.

MEW is solvent-free, unlikely SES, making it more biocompatible and applicable in more medical fields [52, 56]. MEW scaffolds allow cell attachment, proliferation, and the formation of the extracellular matrix since these scaffolds have a controlled porosity that facilitates rapid and homogeneous infiltration by cells [49, 55].

This method makes using thermoplastic materials viable, especially suitable for processing biocompatible polymers [6]. A high viscosity and low conductivity fluid results in a straight melt

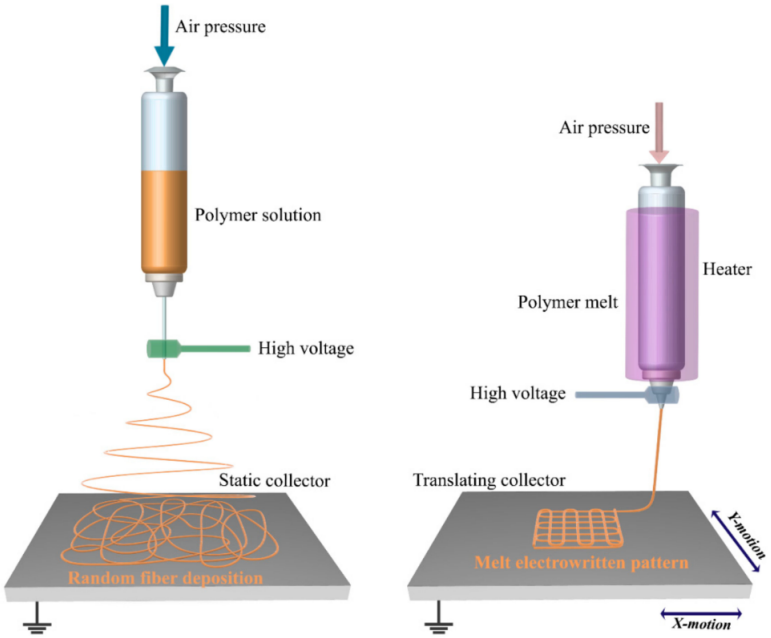

Figure 3.4: Schematic representation of SES (left) and MEW (right) fiber deposition [35].

flow. This electrified jet will cool and solidify into a defined position, and since it lacks residual solvent, it's possible to print layers upon other layers [49].

3.3.3 Use of MEW for POP Repair

MEW allows using different biocompatible and biodegradable materials, making this technique useful in several applications of Tissue Engineering [35]. Despite this wide range of applications, there is still an insufficient number of studies on the development of MEW biodegradable meshes intended for POP repair [4].

Ren et al. [4] developed composite meshes using MEW for POP repair applications by using PCL and Polyethylene glycol (PEG), two biodegradable polymers, approved by the FDA for medical devices. Their goal was to test the effect of the material, mesh geometry (by adjusting the spacing between filaments), and mesh state. To do that, they performed tensile testings, degradation tests, antibiotic and antimicrobial tests, and biocompatibility tests.

The authors concluded that composite meshes degrade faster than PCL, which means it's possible to change the ratio PCL:PEG and obtain a mesh that will have the same rate of degradation as the rate of regeneration of the pelvic tissue. Considering the % of mass loss, in physiological conditions, the higher the PEG content in the fibers, the higher the % of mass loss. Regarding mechanical testing, the authors concluded that the composite meshes presented higher strength than PCL scaffolds. The same applies to the stiffness of the meshes; the higher the content of PEG, the higher the stiffness. The mesh geometry (mesh spacing of 1 mm or 1.5 mm) did not significantly impact the tensile strength. Since PP-based meshes increase the risk of infection and inflammation in women, the authors also incorporated antibiotics and tested the effect of different dosages [4].

Besides all the possible new studies that can be performed (using different geometries, different dosages of antibiotics, and/or different ratio PCL:PEG), Ren et al. [4] concluded that it is possible to produce a biodegradable mesh, via MEW, that can be adjusted to the desired mechanical properties and, if required, incorporate antibacterial properties with slow releasing into the meshes. This type of mesh can be used to treat women with POP without providing the withdrawal of PP-based meshes.

3.4 The Use of Antistatic Agents in Melt Electrospinning Writing

Antistatic agents are "soap-like" molecules [8, 57] with an amphiphilic nature, meaning they have both hydrophobic and hydrophilic properties. On one hand, they have a hydrophobic side interacting with the material's surface (being compatible with it). On the other hand, they have a hydrophilic part [58], made of fatty acid esters, ethoxylated amine, and phosphate esters that migrate to the surface [8], attract the air moisture and bind the water molecules [45, 58, 59].

Antistatic Agents Classification

There are two types of antistatic agents: internal and external. These two categories differ when the agent is "introduced" in the material. Internal agents are mixed with the polymer during the process, meaning they must be compatible with the polymer and stable during manufacturing. This type of additive continually migrates to the surface of the polymer to form a thin film without altering the surface appearance [58, 59].

External antistats are applied when the polymer is already manufactured, usually by an aqueous or alcoholic solution, meaning that they can be easily eliminated through handling. Because of that, external antistats are ideal for short-term applications [58, 59].

3.4.1 Effects of Antistatic Agents on the Melt-Electrospun Fibers

Additives like antistatic agents are a powerful tool to prevent electrostatic build-up on materials that generally lead to dust accumulation and electric shocks [8, 60]. These antistatic agents will absorb water and ions from the air and form a continuous layer of water on the additive's surface. This will increase the number of ions on the surface, improving the surface conductivity of the material [8].

During MEW printing, the material will be pushed towards the collector by the electrostatic forces generated by the electrical field, which can compromise the processability of the material. Antistatic agents will improve the processability of the material, as well as the surface ionic conductivity, which can result in a reduction of the fiber diameter [57]. Besides that, these additives improve the charge's distribution on the material surface, resulting in a more stable and controlled jet that will stretch uniformly, leading to thinner fibers [8].

Sheoran et al. [45] studied the influence of Hostastat® FA 38 (HT) [61] on the ionic conductivity of PP. To do that, they used the MEW technique for printing the fibers and mixed PP with the antistatic agent at different weight percentages (wt%) values.

HT was mixed as a dilute ionic supplement with two formulations of linear low-density polyethylene (LLPDE) polymers at wt% values of 0, 0.1, and 5. Results showed that the melt conductivity of the polymer increased by $20-40\times$ (depending on the type of LLPE) at 5.0 wt% of HT. The authors also measured the viscosity level of both LLPDE and concluded that it didn't decrease more than 20%. All other properties didn't suffer any significant change [45]. However, in the scope of this dissertation, it is important to note that even though a 5.0 wt% of HT provides the best results in melt ionic conductivity, it's necessary to evaluate the cytotoxicity of the meshes for POP repair.

Sheoran et al. [45] concluded that ionic conductivity is an essential characteristic that affects electrospinning outcomes and the role that viscosity and conductivity have in the fiber diameter. Lastly, they concluded that incorporating an antistatic agent like HT at a low doping level could increase the ionic conductivity of the material and decrease the fiber diameter.

Chapter 4

Materials and Methods

This chapter details the materials and methods used to achieve the final goal. It begins with an overview of the methodology, followed by the properties of the materials and a description of the methods used. Finally, it presents all relevant instruments and tools.

4.1 Methodology Overview

Figure 4.1 shows an overview of the methodology followed based on the protocol presented in [57].

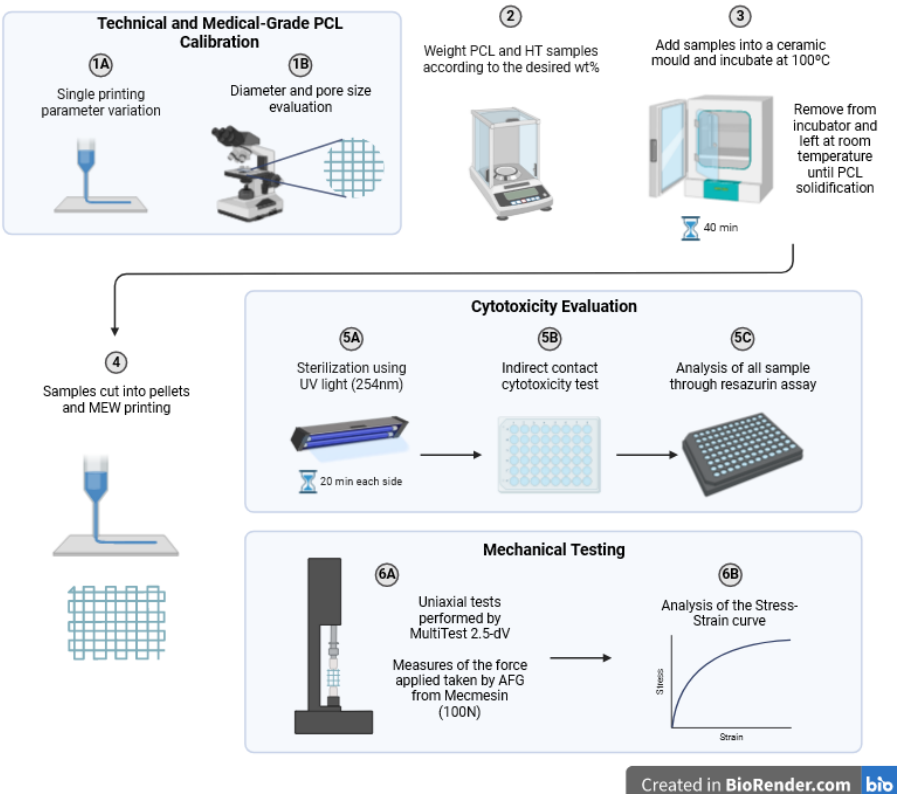

Figure 4.1: Schematic representation of the methodology followed during the dissertation.

Firstly, the MEW prototype was calibrated for technical and medical-grade PCL to ensure the meshes have the desired diameter (steps 1A and 1B). After that, the polymer was melt-blended with the additive at different wt% (steps 2 and 3). Having the resulting pellets, the meshes were printed using the MEW technique (step 4).

Lastly, cytotoxicity tests were performed to evaluate if these meshes were suitable for POP repair or if they were too toxic for the cells (steps 5A, 5B, 5C), as well as uniaxial tensile tests (mechanical testing) to evaluate the mechanical properties of these meshes (steps 6A and 6B).

4.2 Materials

This section outlines the materials used to fabricate the desired meshes. Detailed information about each material, including its properties and relevance to the study, is provided below.

4.2.1 Polymer

PCL is a nontoxic [52, 62] biodegradable polyester polymer that lacks bioactivity [7, 63] and is very popular as a base polymer for long-term drug-delivery applications [62] due to its long degradation period and superior rheological and viscoelastic properties [52].

PCL is a hydrophobic polymer, meaning it is not soluble in water or other solvents. Printing a PCL scaffold using a solution-based printing technique, like SES, implies the removal of the solvent after the printing process. However, using MEW to print PCL scaffolds avoids this challenge, as the polymer is melted and extruded directly onto the substrate without solvents. This makes MEW an ideal printing technique for PCL, offering precise control over scaffold architecture and properties [64]. PCL is the gold standard used in most studies for MEW processes [65].

PCL presents a variety of features that are appealing in biomedical applications, such as processability, mechanical properties, and high biocompatibility [56]. It has a low melting temperature (58 - 60ºC) [52, 66], fast solidification, great malleability, 3D printing capacity, heat molding, and shape memory [66]. Moreover, PCL has been approved by the FDA for human use [67, 68].

The degradation rate is an essential material characteristic when considering a Tissue Engineering application. In the case of POP repair, the material's degradation rate is expected to match the tissue's regeneration rate. If degradation is slower than tissue regeneration, it will delay tissue growth. Conversely, if it is faster, a loss of connection between the tissue and the scaffold will occur, leading to a delay in the healing process [68]. Typically, PCL degrades after 2 to 3 years [62], but its degradation rate can be manipulated by changing its molecular weight and crystallinity or even by modifying its structure [63], though this depends on the properties of the PCL scaffolds such as porosity.

Specifically for biomedical applications, the most widely studied polymer is medical-grade PCL, which has a higher purity than technical-grade PCL and produces the highest printing quality. With medical-grade PCL, the designs are executed with more control and accuracy than with technical-grade PCL [7]. However, medical-grade is more expensive than its technical-grade counterpart.

Medical-grade PCL has already been used in a large number of FDA-approved medical devices, and it has been showed that, unlikely PP-meshes, it doesn't increase local stiffness and enhance the biomechanical properties of regenerated tissue [29].

In this dissertation, both technical and medical-grade PCL were used. Technical-grade PCL is commercially available as a filament and is sold by 3D4Makers [69]. The version used was Facilan™ PCL 100, which has a filament diameter of 1.75 mm, a density of 1.1 g/cm^3 (ISO 1183), and a melting point of 58 - 60ºC. Medical-grade PCL is commercially available in pellets and was obtained from Corbion [70], under the trade name PURASORB® PC 12 polymer. This polymer must be stored at -15ºC to maintain its original properties for five years. It retains its properties if stored at room temperature in the original package for a year.

4.2.2 Antistatic Agent

The antistatic agent used during this dissertation was the Hostastat® FA 38 (HT), available commercially by Clariant [61]. This antistatic agent was designed to be properly mixed with thermoplastics, avoiding any chemical incompatibility between the melt polymer and this additive [45].

It is possible to read on its technical sheet, available in [61], that HT is an ethoxylated alkyl amine based on renewable fatty acid, with dripping point of 97ºC. According to the seller, this additive is a highly effective internal antistatic agent for polymers, and its main application is to equalize or reduce static charges on the polymers' surface, that can lead to hazardous effects.

This additive should not be stored at temperatures higher than 30ºC, and its shelf life is two years from the shipping date. Furthermore, in the product's technical sheet, the sellers grants its long-term efficiency, high performance, and easier processing.

4.3 Methods

This section details the methodologies employed in the experimental procedures.

4.3.1 Melt-Blending

Melt-blending is the preferred method for creating homogeneous mixtures of different polymers or polymers with additives. By melting the polymer and additive together and then mixing them, it is possible to obtain a homogeneous material. This method allows for the enhancement or modification of the mechanical properties of the resulting material [71]. Since PCL was obtained in the form of pellets and the antistatic agent in the form of powder, it was necessary to use this technique to blend them and get a homogeneous product.

Previous studies [57] have already examined the influence of different wt% concentrations (0.1, 0.5, and 1 wt%) of HT blended into PCL. It was concluded that 0.1 wt% was still toxic to cells but provided a 30% reduction in filament diameter. However, the authors used a pellet to test the cytotoxicity. We will use the final product, the mesh, so the induced cytotoxicity may be lower since the mesh is much thinner than the pellet.

Therefore, it was decided to use 0.03, 0.06, and 0.1 wt% of HT to evaluate the effect of the additive on the fiber diameter while seeking a non-toxic option for printing thin fibers. It was used medical-grade PCL, weighing 12.0424 g, and placed onto griffin beakers lined with aluminum foil. By using Equation 4.1 and knowing the mass of PCL used, it's possible to calculate the weight of HT needed: 0.0036, 0.0072, and 0.0121 g for 0.03, 0.06, and 0.1 wt%, respectively. Three samples were prepared for each concentration.

$$wt = \frac{m_{HT}}{m_{HT} + m_{PCL}} \times 100 \iff m_{HT} = \frac{wt \times m_{PCL}}{100 - wt} \tag{4.1}$$

After all the measurements, the samples were incubated at 100ºC for 40 minutes in a Drying Oven VWR® VENTI-LINE® with forced convection (Figure 4.2). Then, the beakers were removed from the incubator and left at room temperature until PCL solidification.

Figure 4.2: Samples inside the Drying Oven VWR® VENTI-LINE® for melt-blending the material.

After solidification, the samples were removed from the beakers and separated from the aluminum cover. They were also cut into small pieces to be inserted into the pellet extruder afterward.

4.3.2 Uniaxial Tensile Testing

Tensile tests are a helpful tool for studying the mechanical properties of materials since they allow us to determine how materials behave under tension load. In this type of test, the material is submitted to tension to find out how strong it is and how much stretched it can be before it ruptures [72]. Usually, uniaxial tensile tests assess mesh properties like stiffness [73].

Considering Equations 4.2 and 4.3 [72], and knowing the force, F (N), that is applied to the sample, its initial, I_0 (mm), and final lengths, I (mm), and its area, A (m^2), it is possible to represent the Stress-Strain Curve of that material and, with that, calculate mechanical properties of the material, like tensile strength or Young's Modulus [72].

$$\sigma = \frac{F}{A} \, (N \cdot m^{-2} = Pa) \tag{4.2}$$

$$\varepsilon = \frac{(I - I_0)}{I_0} \tag{4.3}$$

Figure 4.3 represents a typical Stress-Strain Curve, in which it is possible to obtain much information about the material's properties. Elastic deformation means that the deformation of the material can be reversed by removing stress. In a Stress-Strain Curve, this can be identified by the initial linear section of the graph (in which the stress, σ, is proportional to the strain, ε) [74].

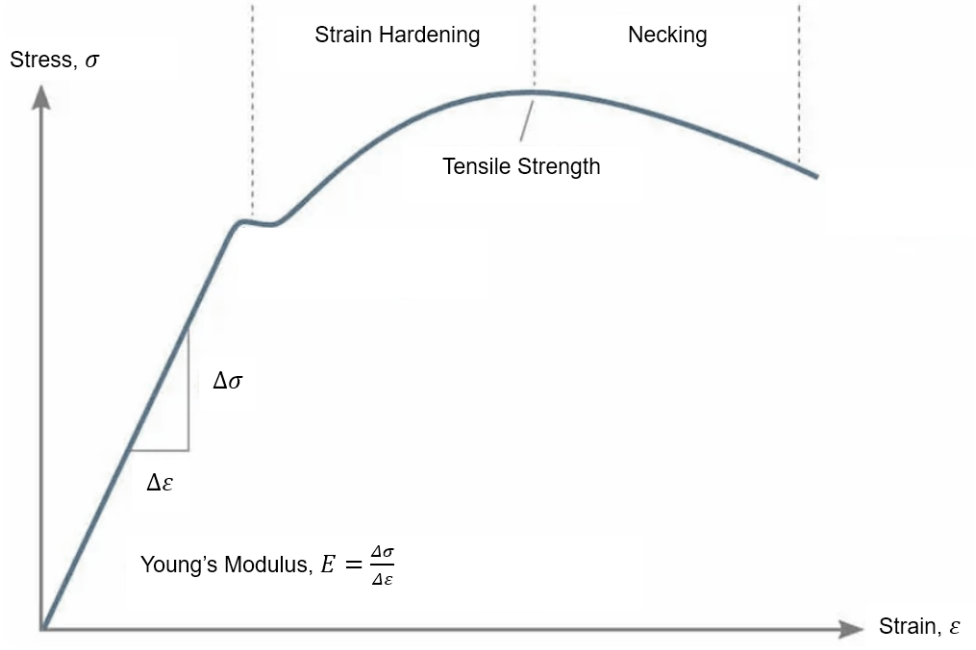

Figure 4.3: Schematic of a typical Stress-Strain curve.

Young's Modulus (or elastic modulus) represents the ratio of stress to strain under elastic deformation (Equation 4.4 [74]). It indicates the material's resistance to deformation when subjected to a force and is determined by the initial slope of the stress-strain curve [74]. Young's Modulus is a measure of a material's stiffness.

$$E = \frac{\Delta\sigma}{\Delta\varepsilon} \, (Pa) \tag{4.4}$$

4.3.3 Cytotoxicity Evaluation

A cytotoxicity evaluation allows one to evaluate the living cells' reaction to the biomaterial in a cell culture assay, giving insights into both cell viability and the ability for cellular growth [75].

There are two types of Cytotoxicity Assays: Direct Contact Assay and Indirect Contact Assay. The first one mimics the direct interaction between the mesh and the cells. However, in this case, we were not interested in whether the geometry would allow for cell adhesion and proliferation; we

only wanted to know the meshes' cytotoxicity. Therefore, an Indirect Contact Assay (according to ISO 10993-5:2009) was chosen, which consists of replacing the cell medium with the material medium. In this way, the cells would be in indirect contact with the material, allowing us to infer the cytotoxicity of the material.

Samples Sterilization

Biomaterials that are intended to be used in the field of medicine must be sterile. Sterilization can be performed via physical and/or chemical methods and is defined as a process that eliminates all forms of microbial life [76, 77]. This term is commonly mixed up with disinfection, which is a process that eliminates all pathogenic microorganisms, except bacterial spores [76].

Ultraviolet (UV) light is commonly used to sterilize polymers due to its simplicity and low-cost procedure. This method is known for having a strong antimicrobial activity but a poor penetration into solids, which may alter the polymer molecular weight, chain length, and chain termination [78]. Ethanol (EtOH) is commonly used to disinfect bioresorbable electrospun polymers that will be seeded with cells in culture. To disinfect the filaments, it is only necessary to soak them in EtOH and then wash them with phosphate-buffered saline solution or with a culture medium [79]. Since EtOH soaking is a disinfection treatment, it needs to be combined with a sterilization technique to eliminate the remaining bacterial spores. Effective sterilization can be assured by disinfecting the samples with EtOH solution and then sterilizing them with UV radiation [80].

In this study, two different paths to obtain sterile meshes were chosen. One set of samples was sterilized by exposure to UV light (254 nm) for 30 minutes (termed as UV samples). The other set was disinfected by immersion in a 70% EtOH bath for 20 minutes, washed with Phosphate-Buffered Saline (PBS) for 5 minutes (3 times), followed by sterilization by UV light for 30 minutes (termed as ET + UV samples). All the mesh samples were obtained with a circular punch of 8 mm and identified according to their sterilization method and wt% of HT.

Cell Culture

Human neonatal dermal fibroblasts (hNDFs) isolated from human neonatal foreskin samples (Coriell Institute for Medical Research, USA) were cultured in Dulbecco's Modified Eagle Medium (DMEM) supplemented with 10% fetal bovine serum (FBS, Gibco), antibiotics (1% v/v of both penicillin/streptomycin and amphotericin B (Sigma-Aldrich)). Cells were cultured in 5% CO_2 at 37ºC in tissue culture polystyrene flasks.

For transferring the cells to the 24-well plate, cells were trypsinized when reaching 80% confluence using 0.05 wt% trypsin/ethylenediamine tetraacetic acid (EDTA) solution (Sigma-Aldrich) and centrifuged at 1200 rpm for 5 minutes.

Metabolic Activity Evaluation

The metabolic activity of the cells can be evaluated by a resazurin assay. This assay uses resazurin, a cell-permeable dye that is blue, non-toxic, and weakly fluorescent. When in contact with the

resazurin, the active cells will reduce it to resorufin, which is pink and highly fluorescent. By reading the emitted fluorescence (proportional to the number of active cells), we can estimate cell viability in an accurate way [81].

Initially, the meshes' samples were placed in a 24-well plate for sterilization, as shown in Figure 4.4.

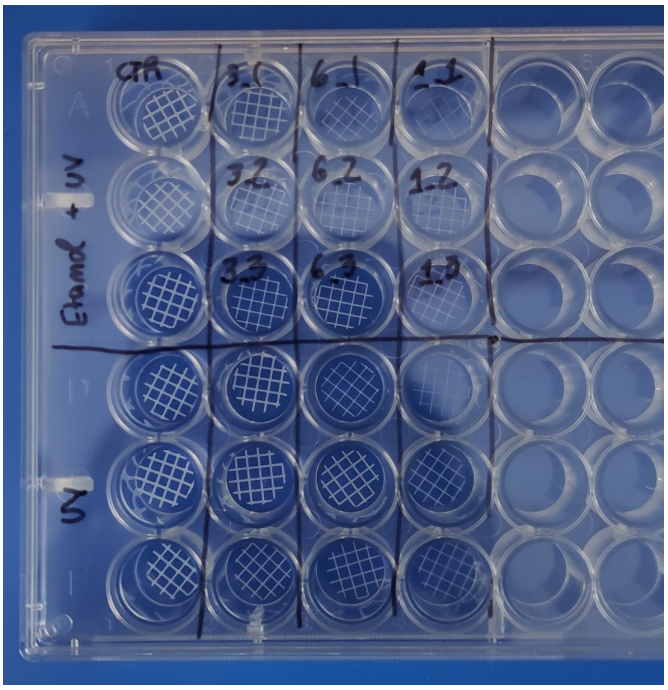

Figure 4.4: Samples placed in a 24-well plate, identified by HT concentration and sterilization method.

The cells were seeded in a treated 24-well plate (4×10^4 cells/400 μL DMEM) and cultured for 24 hours. The meshes' samples were transferred to Eppendorfs (2 mL) with culture medium and incubated for 24 hours. After this time, the medium in contact with the cells was replaced by the one in contact with the meshes, and the resulting samples were again incubated for 24 hours.

To evaluate the metabolic activity, the medium from these samples was transferred to a black 96-well plate. From each well, we collected three samples of medium for the resazurin assay, which means that for each concentration, we had nine values for the metabolic activity evaluation.

The black 96-well plate was incubated in DMEM containing 20% (v/v) resazurin sodium salt (Sigma-Aldrich) for 2h at 37 ºC, and the fluorescence was measured using a microplate reader (Synergy MX, BioTek) at 530 nm (excitation) and 590 nm (emission). Having the value of fluorescence on each well, it is necessary to remove the baseline fluorescence of the resazurin, and then, by calculating the mean of the resulting values, we obtain the mean cell activity that each concentration of HT provides.

4.3.4 Statistical Analysis

There are two different types of statistical analysis that are appropriate for continuous data: parametric and nonparametric tests. Parametric tests are suitable for large datasets that follow a normal distribution. Usually, the mean value is an accurate representation of the center of the distribution of the data. Nonparametric tests are suitable for any continuous data and are independent of the scale and data distribution. In this case, the median would be a better representation of the center of distribution of the data. Furthermore, this type of test is suitable for any dataset size [82].

The data available for the resazurin assay was presented as metabolic activity. The statistical analysis of the data was performed using the one-way analysis of variance (ANOVA), and the comparisons between different HT concentrations and sterilization methods were evaluated through the nonparametric Mann-Whitney U test. The statistical significance was considered for a $p < 0.05$. For each condition, a minimum of three specimens were considered.

4.4 Instruments and Tools

This section provides an overview of the instruments and equipment utilized in the experimental procedures.

4.4.1 G-Code

Geometric Code, or G-Code, is a programming language for Computer Numerical Control (CNC) machines. G-Code allows automation of the movement, precision, and control of CNC machines since it is embedded in their software. This language allows the control of the movements of these machines: where to move, how fast to move, and which path the machine should follow. This way, a 3D printer will be instructed where to deposit material, layer-by-layer, and an object with a precise geometric shape will be formed [83]. The standard structure of a G-Code line is:

G## X## Y## Z## F##

The first part of this structure is the G-Code Command (G). The second part represents the coordinates (X, Y, Z) we want the machine to move. The third part sets the feed rate, which means the speed of the movement (F) [83]. Some of the most important commands are listed below.

- **G21/G20** - sets the units to millimeters or inches, respectively. This parameter must be defined at the beginning of the code. If it's not specified, the program will use the units from the previous program.
- **G01** - instructs the machine to move in a straight line at a given feed rate until it reaches the coordinates given.
- **G02** - instructs the machine to move clockwise in a circular pattern. In this case, it's necessary to define the center of rotation and deviate from the standard format. An example of a

typical line of this command is G## X## Y## I## J##. Here, X and Y are the end position coordinates, and I and J are the offsets of the center point (the relative coordinates of the center point to the current one).

- **G17/G18/G19** - these commands are used to select the working plane of the machine. G17 is for the XY plane, G18 is for the XZ plane, and G19 is for the YZ plane.
- **G28** - this command is used to move the tool to its reference point. If, along that path, the machine collides with some structure, it's possible to indicate the coordinates of a known intermediate point by adding the X, Y, or Z coordinates after G28.
- **G90/G91** - using the machine in an absolute or relative mode is possible. This means that, in absolute mode (G90), the positioning of the tool is always from zero/origin. In relative mode (G91), the positioning of the tool is relative to the last point.

FullControl GCODE Designer

The G-Code software chosen to design the desired meshes was the "FullControl GCODE Designer" [84]. During this dissertation, the Excel sheet version of FullControl, present in Figure 4.5, was used (Excel is a front-end of a Visual Basic application).

This software already includes standard features, such as lines or circles. To design the mesh, the user only needs to write the initial and final coordinates of specific movements (in the case of a cartesian line), the extrusion, and the desired movement speed. It's also possible to choose between "Print" and "Travel" to indicate if the user wants the material to be extruded during that movement. Besides that, the user can also set different printing parameters, such as the temperature.

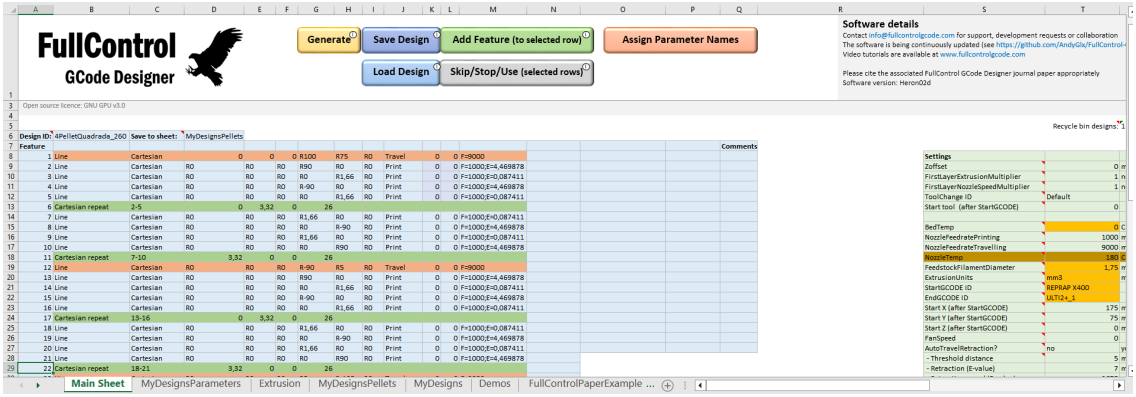

Figure 4.5: Main Excel sheet of the software FullControl GCODE Designer.

NC Viewer

FullControl GCODE Designer doesn't allow to visualize the output of the G-Code, so in this dissertation, the web application NC Viewer [85], present in Figure 4.6, was used to perform that

task during the design of the different meshes. This application also allows one to visualize the meshes from different points of view.

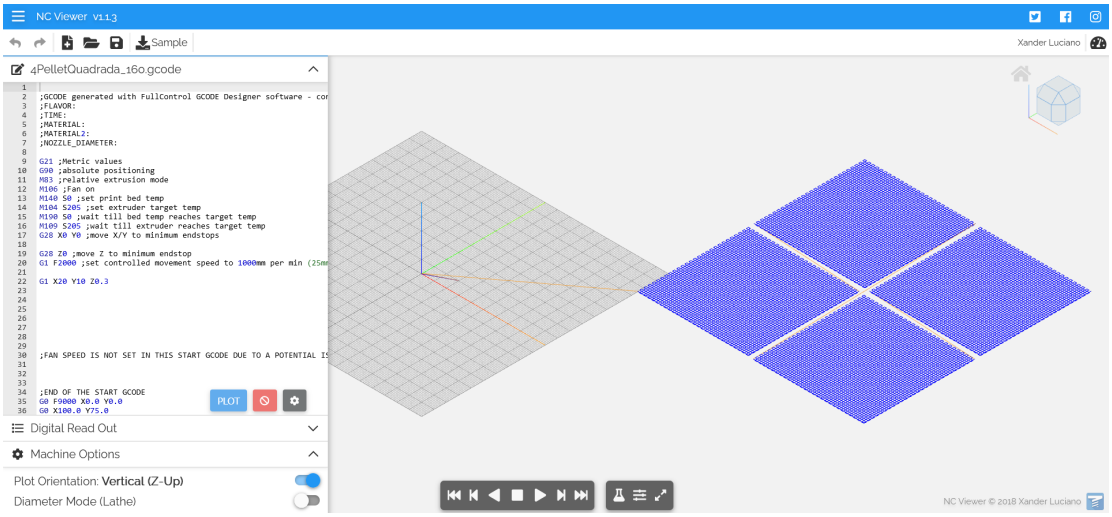

Figure 4.6: NC Viewer output of a four square meshes G-Code.

4.4.2 MEW Prototype

The MEW prototype used during this dissertation (present in Figure 4.7) was developed under the scope SPINMESH, funded by FCT. It was built with a modular architecture based on the different functions of each component, including structure, control, movement, heating, material supply, material collection, and a high-voltage generator. This generator was purchased from a biomedical equipment supplier called Linari Engineering, Italy, and has a range of 60 kV - 150 W and a minimum output current of 0.01 mA [2].

The main components are the stepper motors, the heating and supplying parts, and the controller board (which reads the inputs and generates the outputs, controlling the machine's movements). The controller board chosen was the Duet 3D 2.0 Ethernet because it allows using several extruders [2].

The device was built using an XY moving collector (whose movements are guaranteed by linear actuators driven by the stepper motors [2]) and a Z moving printing head (maximum height of 70 mm) [27]. The collector is a square-shaped aluminum plate with a 3 mm thickness and an area of 270×270 mm^2 [2]. The positive voltage is applied to the collector and the negative to the nozzle, leading to a uniform electrical field that allows MEW printing [27].

The difference between the feeding system of this printer and the traditional electrospinning systems is that, in this case, the fibers are deposited in a flat or cylindrical collector. Here, the polymers are fed with a screw extruder (Bondtech QR) that will allow continuous feeding at a controlled rate. This system provides stability and a precise feeding rate of small volumes of polymers [2].

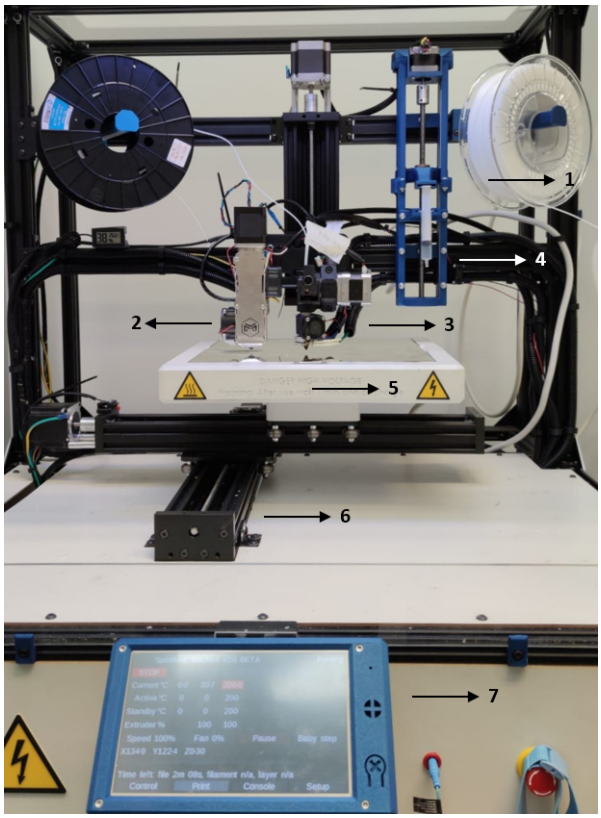

Figure 4.7: MEW prototype developed at Laboratório de Desenvolvimento de Produtos e Serviços (FEUP). 1 - Technical-grade PCL filament; 2 - Pellet extruder; 3 - Filament extruder; 4 - Syringe; 5 - Moving collector; 6 - Linear actuators; 7 - LCD touch screen.

This printer has two interfaces for the user: one LCD touchscreen and a web interface. In both, the user can monitor the equipment's parameters and control which jobs are being printed [2].

4.4.3 Uniaxial Tensile Testing

To conduct the uniaxial tensile tests described earlier, the MultiTest 2.5-dV device was used [86]. This equipment facilitates motorized force testing.

A force gauge was also used to measure the force during the push/pull test (in this case, only pull tests were done). The load cell used was the Advanced Force Gauge (AFG) from Mecmesin, with a capacity of 100 N (since it gives more precise results than a 2500 N one). This AFG was connected to the computer with the software VectorPro MT from Mecmesin, which allows for the collection of all the measured data (load applied to the mesh, displacement of the folds, and time).

Figure 4.8 shows both equipment, used during the uniaxial tensile testing process.

4.4.4 ZEISS AxioPhot Microscope and Stream Basic software

To correctly measure the diameter of every printed mesh, ZEISS AxioPhot Microscope and the Stream Basic software were used. Stream Basic software allows one to visualize the mesh in live

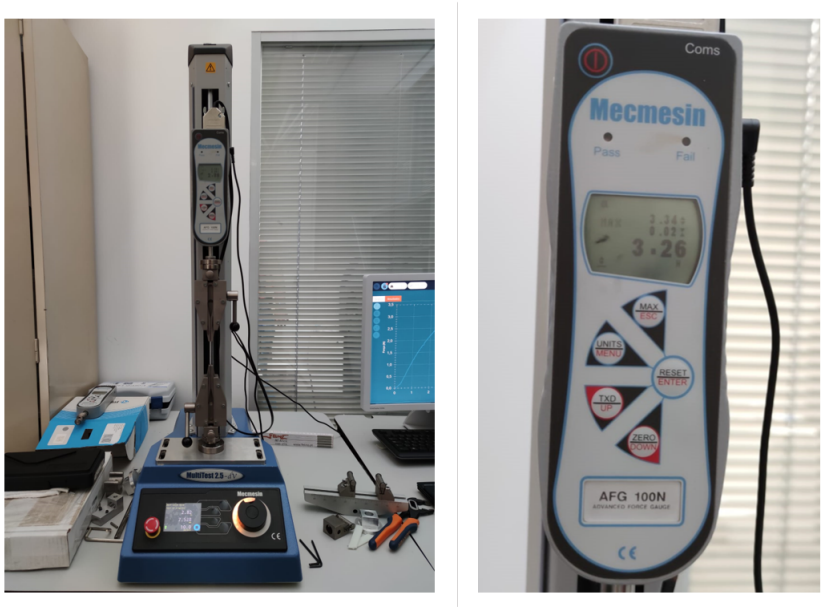

Figure 4.8: Equipment used to perform the uniaxial tensile tests: MultiTest 2.5-dV (left) and AFG of 100 N (right).

mode and also perform several measurements, like the filament diameter or the pore size. Figure 4.9 presents both the microscope and the software used to the diameters measurement.

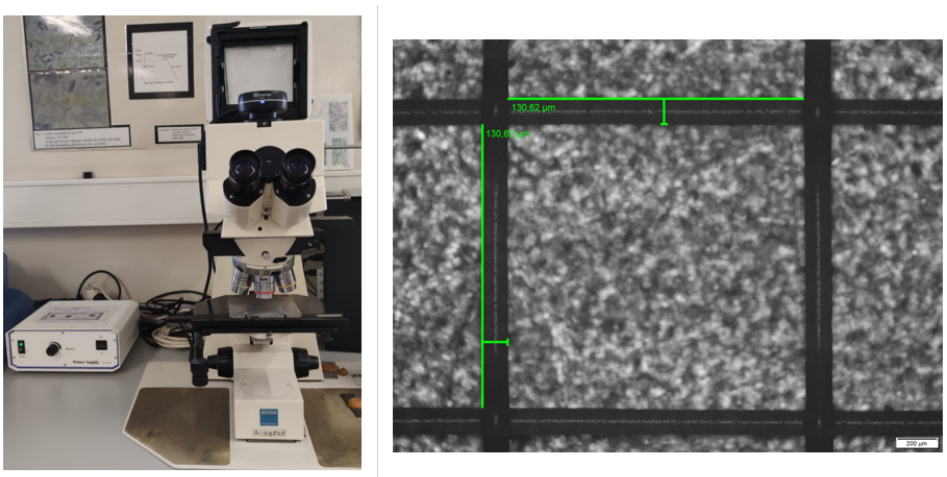

Figure 4.9: Equipment used to measure the meshes' diameter: ZEISS AxioPhot Microscope (left) and Stream Basic OLYMPUS software (right).

Chapter 5

MEW Device Calibration

This chapter will describe the process of designing the meshes and calibrating the MEW device for both technical and medical-grade PCL.

Previous studies [87] have established optimal printing parameters when using the pellet extruder of the prototype. However, recalibration of the device was necessary due to recent modifications. To determine the optimal printing parameters, the device undergoes calibration initially for technical-grade PCL. Subsequently, calibration for medical-grade PCL will follow, with the technical-grade parameters serving as the starting point.

5.1 Meshes Design

For the calibration process, it was chosen to print square meshes with fiber diameters of 160, 200, and 260 μm. It's necessary to adjust the extrusion, E (mm), to print different diameters in the G-Code. Equation 5.1 [87] was used to calculate this extrusion, where $D_{extrusion}$ is the desired fiber's diameter (μm), and $L_{extrusion}$ is the length of the printed filament (mm). $D_{market\,filament}$ is the diameter of the PCL filament, which is 1.75 mm. This equation will be used as a starting point; however, it can be adjusted after calibration to obtain the desired diameters.

$$E = \frac{(D_{extrusion} \times 0.001 \times 1.5)^2 \times L_{extrusion}}{D_{market\,filament}{}^2} \tag{5.1}$$

Square Geometry

The geometry of a square mesh is simple and easy to design. It's only necessary to print a line, then move perpendicular to form the pore and print another line in the opposite direction. Having this process repeated, a sequence of lines equally spaced will be obtained. To form the pore, it's necessary to consider the diameter of the fiber. In this case, a pore size of 1.5 mm was chosen, so in a 160 μm mesh, the lines should be spaced by 1.66 mm.

Sinusoidal Geometry

To design sinusoidal waves, Equation 5.2 was used, where a is the amplitude of the wave; b is its wavelength; c and d shift the wave in the y-direction and x-direction, respectively.

$$y = a \cdot sin(\frac{2\pi}{b} \cdot (x - c)) + d \tag{5.2}$$

Previous studies [33] on different sinusoidal meshes showed that wavy fibers with an amplitude of 1.25 mm and wavelength of 3.5 mm behaved like vaginal tissue when submitted to tension. Since the mechanical tests are uniaxial, a horizontal wave with an amplitude of 3 mm and wavelength of 35 mm was designed to support the vertical waves.

Figure 5.1 shows the design of both geometries, square and sinusoidal.

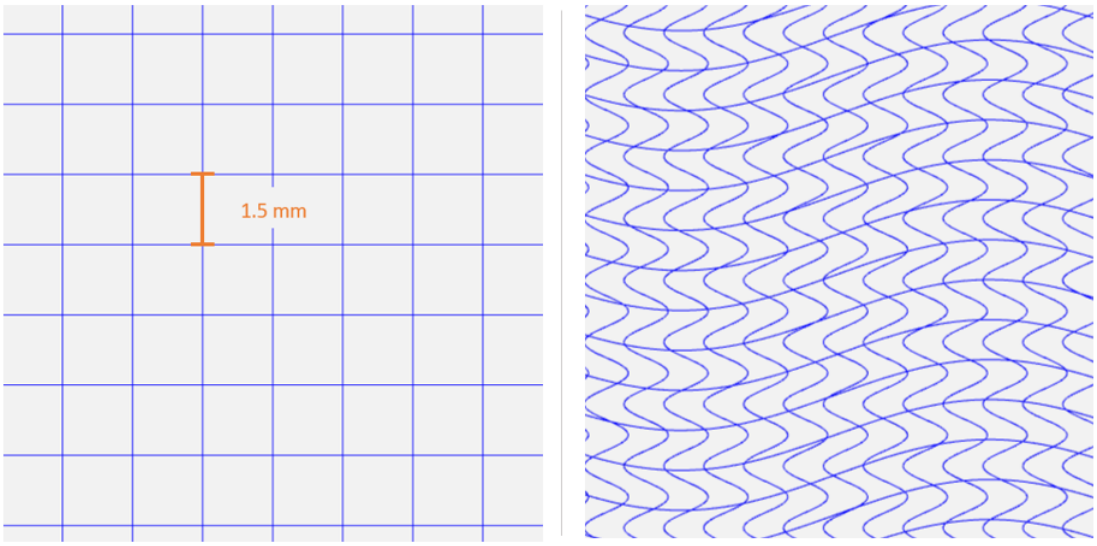

Figure 5.1: Design of a square mesh (left) and a sinusoidal one (right). View from NcViewer.

5.2 Technical-Grade PCL Calibration

In this section, the device calibration for technical-grade PCL was performed. It was chosen to start with technical-grade PCL since it's cheaper than the medical-grade one. It was also chosen to print only square meshes for the calibration to prevent material waste.

Technical-grade PCL is supplied in the form of a filament, so it was cut into small pieces, called pellets, to make it possible to use the pellet extruder. After finding the ideal printing parameters, four meshes of each diameter were printed and measured to perform some final adjustments. These meshes have dimensions of 90×90 μm.

Initial Printing Parameters

The initial printing parameters were chosen based on the results obtained in [87] and are present in Table 5.1. The ideal voltage value obtained in [87] was 6 kV, and after all the modifications, the device can print meshes using voltage values in the range of 3 - 4 kV. As a result of this, the voltage used initially was 3.63 kV. The distance between the nozzle and the collector, also called Z-height, is now fixed at 0.3 mm, so the influence of this distance will not be included as a variable parameter.

Table 5.1: Initial printing parameters used for technical-grade PCL calibration.

Parameters	Temperature (ºC)	200
	Collector's Speed (mm/min)	1000
	Voltage (kV)	3.63

Single Parameter Variation

To perform a correct calibration, a single-parameter variation approach was chosen, focusing on altering the printing parameters, such as temperature, collector speed, and applied voltage, one at a time.

Temperature

The temperature was the first parameter to be optimized, and to do that, all the other parameters presented in Table 5.1 were maintained constant. Table 5.2 shows the values used for each parameter, as well as the variation performed in the temperature.

Table 5.2: Printing parameters used for temperature optimization for technical-grade PCL.

Parameters	Temperature (ºC)	160 - 180 - 200 - 220
	Collector's Speed (mm/min)	1000
	Voltage (kV)	3.63

To test this parameter, it was printed several square-geometry meshes with a diameter of 260 μm. It was observed that:

- 160ºC - Many filaments presented discontinuities and/or accumulation of material.
- 180ºC - There are some discontinuities in the filaments, but less than 160ºC. There are some points of material accumulation.
- 200ºC - A big part of the filaments are well-printed, with only a few point errors.
- 220ºC - The printed meshes are similar to the 200ºC ones, with some punctual errors.

The viscosity of the material is influenced by the printing temperature. In the case of temperatures at 160°C and 180°C, the viscosity remains very high, making it difficult for the material to be extruded continuously. At temperatures of 200°C or 220°C, the viscosity of the material is low. However, to prevent the viscosity from becoming excessively low, a printing temperature of 200°C was chosen.

Collector's Speed

Next, the collector's speed was optimized. In this step, the voltage applied remained constant, and the temperature used was updated according to the best result obtained in the former step. Table 5.3 shows the values used for each parameter, as well as the variation performed in the collector's speed.

Table 5.3: Printing parameters used for collector's speed optimization for technical-grade PCL.

Parameters	Temperature (ºC)	200
	Collector's Speed (mm/min)	500 - 1000 - 1200 - 1400 - 1800
	Voltage (kV)	3.63

To test this parameter, it was printed several square-geometry meshes with a diameter of 260 μm. It was observed that:

- 500 mm/min - Most filaments were curved lines, and the polymer jet was not stable.
- 1000 mm/min - There were fewer deviations in the filaments than before.
- 1200 mm/min - The filaments were straight, without deviations.
- 1400 mm/min - Filaments without deviations.
- 1800 mm/min - There are some discontinuities in the filaments, and many lines are "skipped" (without material deposition).

Having a non-straight filament deposition and an unstable polymer jet are signs of low collector speed (500 and 1000 mm/min). On the other hand, having discontinuities is a sign that the material deposition rate is lower than the collector's speed, skipping some parts of the final product. This means that 1800 mm/min is too high. The only velocities left are 1200 and 1400 mm/min, which allowed us to obtain straight and continuous filaments. However, 1200 mm/min was chosen to ensure that discontinuities would not happen that often.

Voltage

Finally, the voltage applied was optimized. In this step, the temperature and collector's speed used were updated according to the best result obtained in the former steps. Table 5.4 shows the values used for each parameter, as well as the variation performed in the voltage values.

Table 5.4: Printing parameters used for voltage optimization for technical-grade PCL.

Parameters	Temperature (ºC)	200
	Collector's Speed (mm/min)	1200
	Voltage (kV)	2.63 - 3.03 - 3.23 - 3.43 - 3.63 - 4.03 - 4.63

To test this parameter, it was printed several square-geometry meshes with a diameter of 260 μm. It was observed that:

- 2.63 kV - There are several points of material accumulation in the nozzle and, consequently, discontinuities in the printed filament.
- 3.03 kV - There are several points of material accumulation in the nozzle and, consequently, discontinuities in the printed filament.
- 3.23 kV - The polymer jet is stable, and the filament tends to be continuous. Only punctual errors/accumulation of material.
- 3.43 kV - The polymer jet is stable, and the filament is continuous. Only punctual errors/accumulation of material.
- 3.63 kV - The polymer jet is stable, and the filament is continuous. Some punctual errors/accumulation of material.
- 4.03 kV - There are instabilities in the filaments of the meshes.
- 4.63 kV - There are instabilities in the filaments of the meshes, as well as discontinuities.

The voltage applied will determine the material extrusion. If the voltage is too low, it will create a weak electric field that will not be able to extrude all the material, leading to material accumulation (2.63 and 3.03 kV). If the voltage is too high, the electrical field will have such high intensity that it will increase the extrusion speed, leading to points of discontinuity and instability (4.03 and 4.63 kV). This leads us to choose between 3.23, 3.43, and 3.63 kV. To make a safe choice and avoid ending up with an electrical field that is too strong or too weak, a voltage of 3.43 kV was selected.

Diameter and Pore Size Evaluation

As a final step for the calibration, it was necessary to measure all the diameters obtained, as well as the pores sizes. The pore sizes will indicate whether the geometry is correctly printed or not, and the diameter values will indicate if the printer is extruding the right amount of material.

For each sample, it was taken 6 different measures, and the mean value of these measurements is present in Tables 5.5 and 5.6, for the pore and diameter size, respectively.

With these results, it is possible to calculate the mean value for each pore/diameter, calculate the mean error, and analyze. For the diameter values is also possible to adjust Equation 5.1 and calibrate the device.

Table 5.5: Pore size evaluation for technical-grade PCL calibration.

	260 μm	200 μm	160 μm
Sample 1 (μm)	1483.17	1485.11	1520.66
Sample 2 (μm)	1505.40	1562.84	1576.94
Sample 3 (μm)	1527.60	1547.89	1583.67
Sample 4 (μm)	1494.38	1509.51	1624.31
Mean (μm)	1502.64	1526.34	1576.40
Error (%)	0.18	1.76	5.09
Mean Error (%)		2.34	

The pre-defined pore size was 1.5 mm (1500 μm). By looking at the results present in Table 5.5, we can conclude that the mean error is not significant (<10%), which means that the geometry is well-defined.

Table 5.6: Diameter evaluation for technical-grade PCL calibration.

	260 μm	200 μm	160 μm
Sample 1 (μm)	160.00	120.92	91.47
Sample 2 (μm)	144.35	113.74	94.11
Sample 3 (μm)	140.27	117.39	96.67
Sample 4 (μm)	140.18	116.42	100.55
Mean (μm)	146.20	117.12	95.70
Error (%)	43.77	41.44	40.19
Mean Error (%)		41.80	

It was observed that all the diameters had really different values from the desired ones. The mean error obtained was 41.8% which means that the device is not extruding the right amount of material.

Final Parameter Adjustements

Since the device is not extruding the right amount of material, it's necessary to adjust Equation 5.1 so the device can be calibrated. In this case, it's necessary to multiply it by $\frac{100}{100-41.8} = \frac{100}{58.2} = 1.718$, as described in Equation 5.3.

$$E = \frac{(D_{extrusion} \times 0.001 \times 1.5 \times 1.718)^2 \times L_{extrusion}}{D_{filament}{}^2} \tag{5.3}$$

After updating all the necessary G-Codes, new meshes were printed, and their diameters were evaluated, following the same procedures as before. The results are present in Table 5.7.

The meshes have diameters close to the desired ones, presenting a mean error of 4.24%, which can be taken as not significant (<10%).

Table 5.7: Diameter evaluation for technical-grade PCL calibration, after adjustments.

	260 μm	200 μm	160 μm
Sample 1 (μm)	244.05	190.55	156.47
Sample 2 (μm)	242.59	189.51	157.59
Sample 3 (μm)	242.01	189.33	156.53
Sample 4 (μm)	255.72	192.37	152.80
Mean (μm)	246.09	190.44	155.85
Error (%)	5.35	4.78	2.60
Mean Error (%)		4.24	

For every set of meshes, the extruder was refilled so that we were sure that there was a sufficient amount of material in it. Pressure was also applied so that it could enter the nozzle. However, the pellets start to melt once they are put inside the extruder, making it difficult to push down the material. Therefore, the persistent error can be justified by an insufficient amount of material that reaches the nozzle.

5.3 Medical-Grade PCL Calibration

In this section, the device calibration for medical-grade PCL (in the form of pellets) was performed, following the same method as described in the subsequent subsection. The calibration was performed using square meshes, but when the final parameters were found, sinusoidal meshes were also printed to confirm that those parameters were adequate.

Initial Printing Parameters

The initial printing parameters were chosen based on the results obtained for the technical-grade PCL and are present in Table 5.8.

Table 5.8: Initial printing parameters used for medical-grade PCL calibration.

Parameters	Temperature (ºC)	200
	Collector's Speed (mm/min)	1200
	Voltage (kV)	3.43

After visually analyzing the resulting meshes, it was concluded that they were well-printed and similar to the ones obtained during the technical-grade PCL calibration. Therefore, it was not necessary to perform a single parameter variation, passing directly to the diameter evaluation step.

Diameter Evaluation

Similar to what was done in Section 5.2, all the diameters obtained were measured (present in Table 5.9) and will indicate if the printer is extruding the right amount of material. Based on these

results, it is possible to adjust Equation 5.1 and calibrate the device. It was not measured the pore size since the geometry was already calibrated and well-defined.

Table 5.9: Diameter evaluation for medical-grade PCL calibration.

	260 μm	200 μm	160 μm
Sample 1 (μm)	256.05	192.78	157.22
Sample 2 (μm)	239.04	190.89	159.31
Sample 3 (μm)	244.30	190.08	158.31
Sample 4 (μm)	240.20	190.50	158.85
Mean (μm)	244.90	191.06	158.42
Error (%)	5.81	4.47	0.99
Mean Error (%)		3.75	

By analyzing Table 5.9, we concluded that there was no need to adjust Equation 5.1 since the obtained error was not significant (<10%). After these results, sinusoidal meshes were also printed and measured, obtaining an insignificant error. We concluded that the ideal parameters to print both square and sinusoidal meshes were the ones present in Table 5.8.

The next step is to blend PCL and HT and study the influence of this additive on the diameter of the meshes. Therefore, it's not necessary to print three different diameters since we are only interested in the effect that different wt% of HT have in the diameter. This will also reduce the amount of material used and, subsequently, the costs of this study.

It was also noted that the middle part of the meshes is where the geometry is perfect. All the squares are well-defined and uniform; however, when looking at the corners of the meshes, some deviations can be observed (squares are not equilateral). To solve that problem, there was a redesign of the meshes (Figure 5.2) that would provide perfect and uniform samples, leading to meshes of 35×35 μm that are fully useful, allowing us to not waste material and have uniform samples.

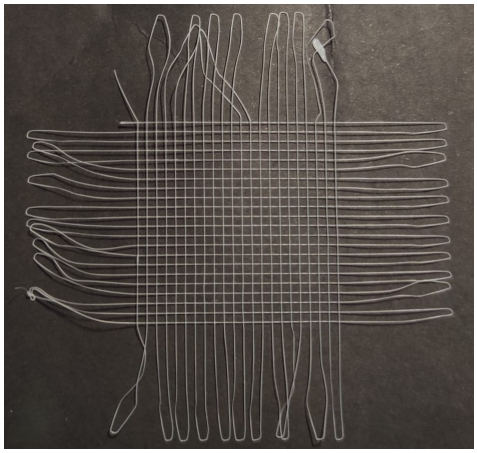

Figure 5.2: Redesign of the meshes that provide uniform samples.

Chapter 6

PCL/HT Meshes: Fabrication and Testing

This chapter describes the process of printing the PCL/HT meshes, as well as measuring their diameters. Then, mechanical tests were performed to evaluate the meshes' behaviour under load, as well as cytotoxicity tests to evaluate the toxicity of these meshes.

6.1 Diameter Evaluation of the PCL/HT Meshes

Since the main goal is to evaluate the additive's influence on the diameter and mechanical properties of PCL, we decided to proceed with this study by only printing meshes with diameters of 260 μm to avoid material waste.

It is also worth saying that before printing all the meshes, some experiments were performed with material from a sample of 0.03 wt%. Then, to perform a systematic evaluation of the HT effect, the extruder was cleaned. However, some residue may have remained, necessitating a new adjustment in the extrusion value (1.5×1.718 in Equation 5.3 was replaced by $1.5 \times 1.718 \times 1.943$). These adjustments led to obtaining control meshes of about 280 μm (instead of the original 260 μm). Instead of re-adjusting, we decided to proceed with the study because the initial diameter was not essential as long as all the control meshes were coherent and had similar diameters (which was verified). Table 6.1 shows the mean diameter values of every sample, as well as the reduction that they provided to the diameter when compared to the control group.

By analyzing the data, we can conclude that the antistatic agent does have the desired effect on the material, allowing it to be more stretched, forming thinner fibers (having a reduction of 65 - 66% in the higher concentration and 14 - 17% in the lower one). Visually, the jet was more stable, and the printed geometries were more uniform than the control ones.

Table 6.1: Diameter evaluation of all wt% samples and calculation of the reduction of the fiber when compared to the control group

	Square Meshes		Sinusoidal Meshes	
	Mean Diameter (μm)	Reduction (%)	Mean Diameter (μm)	Reduction (%)
Control	281.30	-	273.62	-
0.03 wt%	234.04	16.80	234.05	14.46
0.06 wt%	153.92	45.28	165.35	39.57
0.1 wt%	98.41	65.02	95.07	65.26

6.2 Uniaxial Tensile Testing

Tensile tests allow one to visualize how the mesh behaves when submitted to a high load in one direction. In this section, two main evaluations will be performed: how do the meshes behave under load according to their HT concentration; how does the HT concentration affect the mechanical properties of the meshes.

To perform the tensile tests under the same conditions, we created a "model test" in VectorPro software with a minimum extension of 0 mm, maximum extension of 200 mm, and speed of elongation of 10 mm/min. After the test is properly done, the software VectorPro exports the values of load applied and displacement that the folds suffered. To calculate the stress of each mesh, it is necessary to calculate the area of contact between the mesh and the equipment and then divide the load by that area (Equation 4.2). By measuring the initial distance between the MultiTest 2.5-dV folds (I_0), it is possible to calculate the strain using Equation 4.3.

Figure 6.1 presents examples of a square and sinusoidal mesh sample being tested in the MultiTest 2.5-dV equipment with a load cell of 100 N.

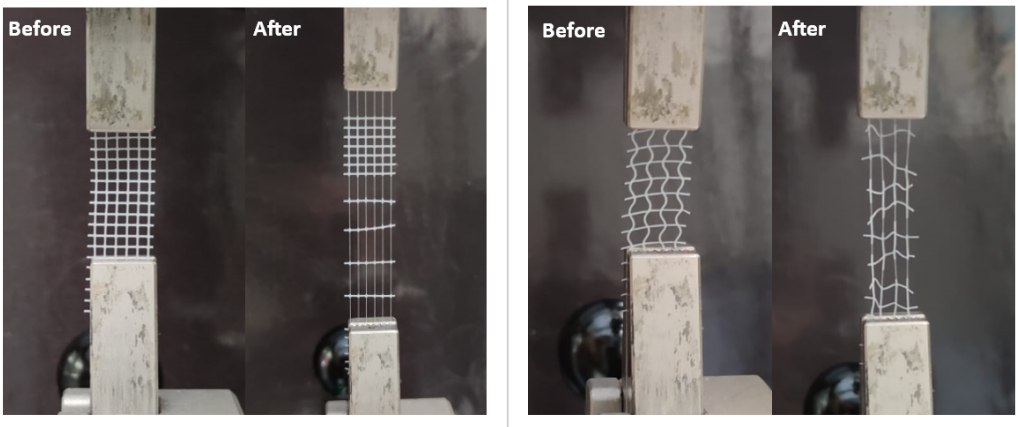

Figure 6.1: Effects of an uniaxial tensile test on a square mesh sample (left) and on a sinusoidal one (right).

HT concentration influence on meshes' behavior under load

For each concentration and for each geometry, seven samples were tested. With the resulting stress and strain for each curve, the mean values were calculated, resulting in the Stress-Strain curves presented in Figure 6.2 for the square (A) and sinusoidal (B) meshes, respectively. The vaginal tissue curve was obtained from [87].

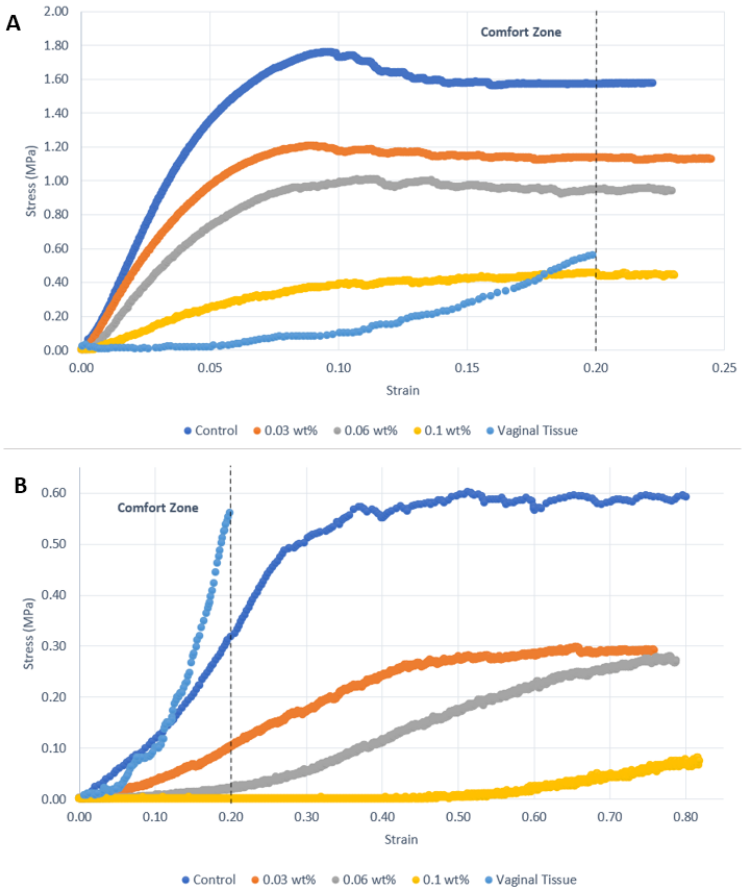

Figure 6.2: Stress-Strain curve of the square (A) and sinusoidal (B) meshes, from all concentrations, and uniaxial stress-strain response of the vaginal tissue.

To correctly analyze these results, it is necessary to introduce two new terms: comfort zone and safety zone, which are associated with the expected strains experienced by vaginal tissue. The comfort zone pertains to stresses encountered during daily activities and has a maximum value of 20% strain. The safety zone relates to high peaks of stress and is set with a threshold of up to 40% strain [1]. The following results will be related only to the comfort zone.

The mesh's geometry will influence the behavior and maximum load supported by the mesh. We can infer that the geometry that best mimics the vaginal tissue behavior is the sinusoidal one, especially the control mesh, which can support similar values of stress up to a strain of 0.15.

The supported load is also influenced by the fiber's diameter (the thicker the diameter, the higher the stress that the mesh can support). By analyzing each graph individually, it is possible to conclude that, independently of the geometry, this statement is true in every curve presented.

Table 6.2 presents the maximum value of stress that each mesh can support (also called tensile strength). These results corroborate this statement as we verify a reduction in the tensile strength value with a reduction in the fiber's diameter caused by an increase in the HT concentration.

Table 6.2: Tensile strength of each mesh within the comfort zone.

	Tensile Strength ± Standard Deviation (MPa)	
	Square	Sinusoidal
Control	1.776 ± 0.128	0.378 ± 0.146
0.03 wt%	1.234 ± 0.348	0.122 ± 0.101
0.06 wt%	1.044 ± 0.132	0.026 ± 0.021
0.1 wt%	0.457 ± 0.101	0.007 ± 0.009

A statistical analysis was also performed to confirm what was previously discussed. We analyzed each curve individually and compared it to its previous wt%. When analyzing the 0.03 wt% curve, we used as control the "Control" (0 wt%) one; to analyze the 0.06 wt% curve, we used the 0.03 wt% as control; and for the analysis of the 0.1 wt% curve, we used the 0.06 wt% curve as control. We did not choose to compare all curves to the Control (0 wt%) curve because if there was a statistically significant difference between that curve and the next one, then the analysis for subsequent concentrations would not give any new insights. In this way, we make sure that every analysis produces a relevant result.

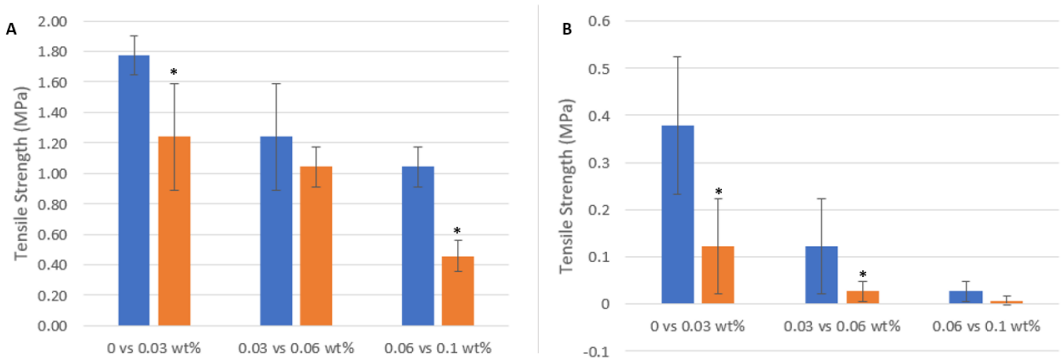

Figure 6.3: Effect of different wt% of HT (Control (0 wt%), 0.03, 0.06, 0.1 wt%) on the tensile strength value for the square (A) and sinusoidal meshes (B). Each group is compared to its previous wt%. *statistically significant when compared with the correspondent control ($p < 0.05$).

Figure 6.3 A and B shows the bar plot of the mean tensile strength and the respective standard deviation for the square (A) and sinusoidal (B) meshes. We can verify that there is a statistically significant difference between all the present groups (meaning that the HT incorporation does have the desired effect of reducing the fiber's diameter) except for the 0.06 wt% square and the 0.1 wt% sinusoidal ones. A detailed analysis proved that in these cases, there were some samples that presented similar or higher diameters than the correspondent control group, which made the

result a non-statistically significant difference. This could have happened due to fluctuations in the voltage supplied during the printing process.

As a final conclusion, as the filament diameter decreases, it is expected that the stress required to induce a specific deformation in the filament will also decrease, which was verified. This occurs due to the increase in the surface area-to-volume ratio, which results in greater sensitivity of the material to external forces applied.

HT concentration influence on the meshes' mechanical properties

To assess if the antistatic agent alters the properties of pure PCL, we can compare the obtained curves (PCL/HT) with curves obtained from pure PCL meshes as long as they have similar diameters and the same geometry. The curves available for PCL meshes were obtained from [87], being square meshes made of medical-grade PCL, with diameters of 240, 160, and 80 μm and a pore size of 1.5 mm. We chose to compare the 0.03 wt% square mesh (234.04 μm) with the 240 μm one and the 0.06 wt% (153.92 μm) with the 160 μm one, due to the similar diameters. It was not possible to compare the curve of the 0.1 wt% mesh (98.41 μm) because its diameter was not close to any available curve. These curves are presented in Figure 6.4.

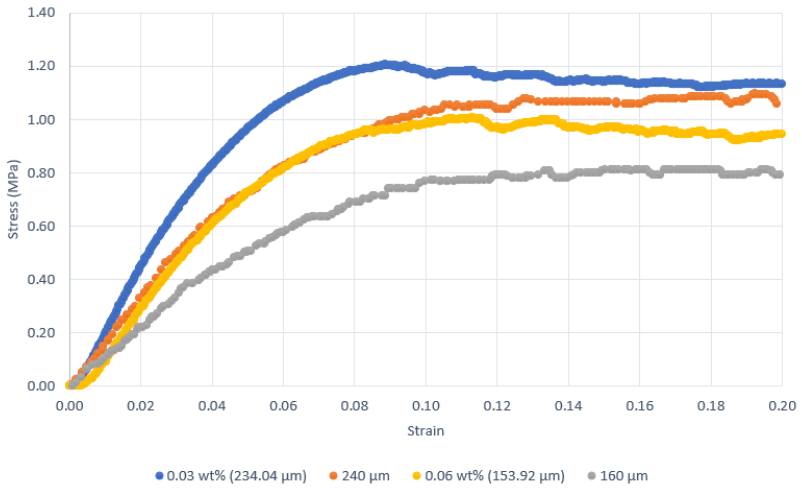

Figure 6.4: Comparison between PCL/HT and PCL square meshes, with similar diameters.

To analyze the influence of each HT concentration on the meshes' mechanical properties, we can calculate the mesh's stiffness and tensile strength. The stiffness of a mesh is a measure of the material's resistance to deformation when submitted to a certain load and can be measured by Young's Modulus (Equation 4.4) value. In turn, tensile strength is the maximum stress that the mesh can support right before breaking, while being stretched. The values of these properties for each mesh are available in Table 6.3.

By comparing the 0.03 wt% curve and the 240 μm one, it would be expected that the pure PCL mesh would support more load, hence having a higher tensile strength value, since its diameter is higher than the PCL/HT mesh. However, we can see that the PCL/HT mesh's tensile strength value is 0.18 MPa higher than the PCL one. The same principle is true when comparing the 0.06

Table 6.3: Comparison of the Tensile Strength and Young's Modulus values between PCL/HT and PCL square meshes.

	Tensile Strength (MPa)	Young's Modulus (MPa)
0.03 wt%	1.234	20.58
240 μm	1.054	14.84
0.06 wt%	1.044	16.15
160 μm	0.813	10.38

wt% curve with the 160 μm one, as the difference between the PCL/HT and PCL tensile strength values is 0.231, being the PCL/HT mesh, the one that supports a higher load while having lower diameter.

It is possible to verify not only an increase in the PCL/HT meshes' tensile strength value but also an increase in the meshes' Young's Modulus values, which means that there was an increase in the meshes' stiffness. The increased tensile strength and stiffness with the incorporation of HT into the meshes suggest that the interaction between PCL and HT modifies the mechanical properties of the PCL.

Zhao et al. [88] developed a polymer-type antistatic agent called TMQ, prepared from isopentenyl polyoxyethylene ether (TPEG), maleic anhydride (MAH) and homemade quaternary ammonium salt (QAS). They mixed TMQ with PP and studied its influence on several properties of PP, including its antistatic, mechanical, and crystalline properties. The incorporation of 15 wt% TMQ in PP resulted in a 38.6% reduction of tensile strength when compared to pure PP. PP surface resistivity was also reduced, which means that the surface conductivity increased. The authors also noticed that the addition of TMQ reduced the crystallinity of the polymer.

Chow et al. [8] studied the effect of different wt% (3, 6, and 9 wt%) of the antistatic agent Irgastat P 18 on the PP/OMMT nanocomposites' mechanical properties. They verified a slight decrease in the tensile strength of PP/OMMT nanocomposites with the increased concentration of additive.

Sun et al. [89] incorporated the ionic antistatic agent Allyl Trimethylammonium Chloride (TMA) in Polymethyl Methacrylate (PMMA) and evaluated its effect on the polymer's properties. A concentration of 1.25 wt% of TMA leads to a reduction in the surface resistance of PMMA 5 times lower than pure PMMA. It was also verified a 38% increase in the tensile strength for the same TMA concentration. The authors also used Acrylic Acid (AA) to improve the compatibility between TMA and PMMA. They concluded that AA increases the polarity of molecular chains, increasing the hydrogen bonding between molecular chains and, therefore, improving the tensile strength of polymers.

The previous studies showed that the incorporation of antistatic agents in polymers modifies the polymer's properties, namely their tensile strength, surface resistivity and polymer's crystallinity. In this study, we verified a tensile strength increase of 17.08% and 28.41% for 0.03 wt% and 0.06 wt% of HT, respectively. There was also a Young's Modulus increase of 38.68% and

55.59% for 0.03 wt% and 0.06 wt% of HT, respectively.

These results suggest that the interactions between PCL and HT promote the hydrogen bondings between molecular chains, and it's possible that the crystallization of the polymer may also be affected. When the crystallization level of a polymer increases, the intermolecular forces are stronger, so the movement of the polymer chains is reduced, and, therefore, the stiffness of the polymer increases [88]. By verifying an increase in Young's Modulus values of the PCL/HT meshes, we can conclude that the polymer's stiffness increased with the HT incorporation, suggesting that the polymer's crystallization was also modified.

As a final conclusion, it is necessary to consider whether is advantageous or not to incorporate HT in PCL meshes. On the one hand, its incorporation will control the charge's distribution on the material surface, resulting in a more stable and controlled jet that is stretched uniformly, leading to thinner fibers. On the other hand, we have seen that this HT incorporation led to a tensile strength and stiffness increase. For the specific case of POP repair, it is ideal to have a mesh that provides good support and can handle high loads while still providing flexibility, avoiding problems like stress shielding.

By observing Figure 6.2 B, we can see that the control mesh supports similar values of stress up to a strain of 0.15. However after this point, the native tissue can support higher values of load. Thus, the slope of the vaginal tissue curve is higher than the control mesh one, which means that the tissue is stiffer than the mesh.

With the right HT incorporation in PCL meshes, we could achieve the ideal mesh stiffness and tensile strength. We already know the HT influence on the fiber's diameter, so we could choose an adequate HT concentration and then adjust the "control diameter" so that, when we print the PCL/HT mesh, we obtain a diameter that supports the same loads as the native tissue. Furthermore, this would increase the mesh's stiffness to the point that the mesh mimics the vaginal tissues' characteristics and behavior. Regarding the stiffness and the stress shielding problem, it is also a fact that, unlikely the synthetic meshes, the PCL ones, will be absorbed after 2 to 3 years of implantation, so even if the mesh is slightly stiffer than the native tissue, it would not be such a problem as it is with the synthetic meshes.

6.3 Cytotoxicity Evaluation

These meshes are designed for the application of POP repair, so it is essential to evaluate not only how they would behave under load but also their cytotoxicity.

As mentioned before, the resazurin assay provides the number of emitted fluorescence that is proportional to the number of active cells. These results are in Figure 6.5, in which each graph (A and B) relates to an independent experiment. These results were normalized to the activity of the cells in the culture medium without any material and sorted by the sterilization method (ET + UV and UV).

Two main topics need to be discussed when analyzing Figure 6.5: within each method of sterilization, which HT concentrations are cytotoxic or not; which method of sterilization provides

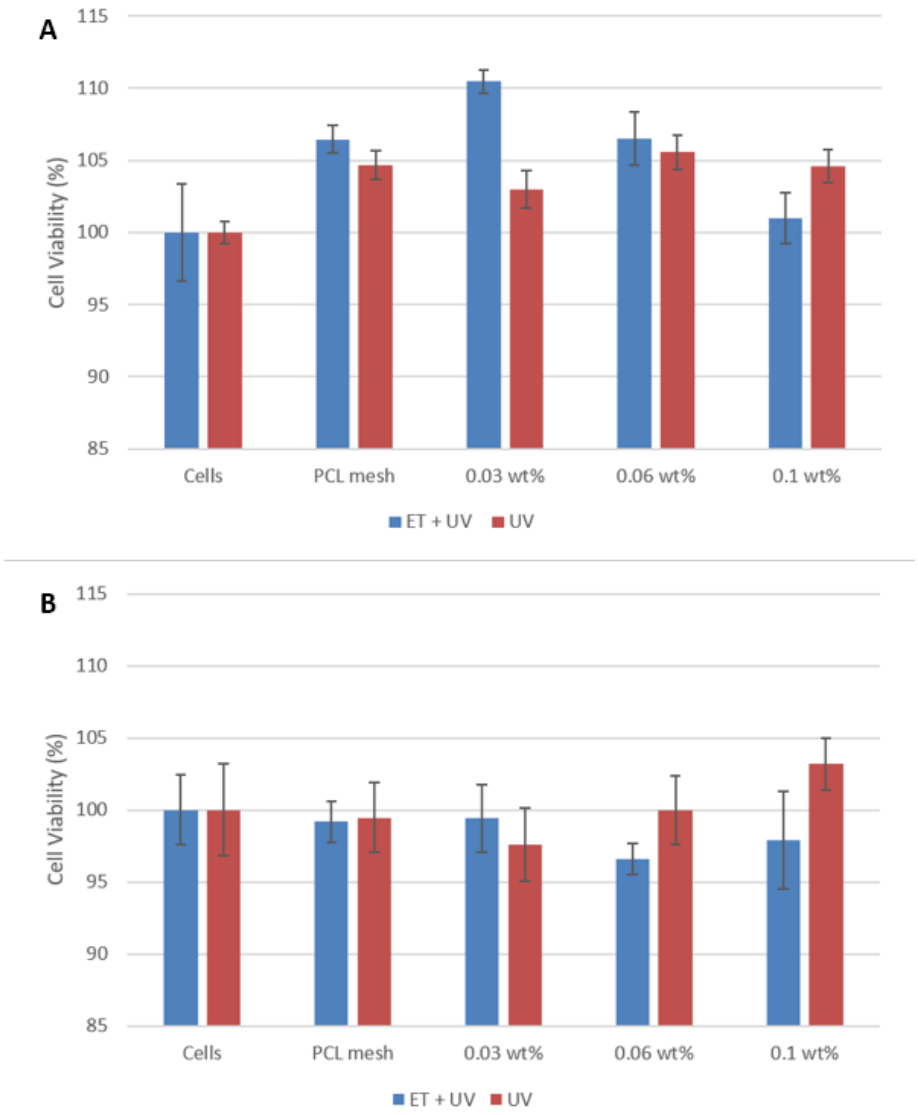

Figure 6.5: Effect of different wt% of HT (PCL mesh, 0.03 wt%, 0.06 wt%, 0.1 wt%) on the cell viability of the dermal fibroblasts with results normalized to the cells in the culture medium (Cells), sorted by the sterilization method. A and B are two independent experiments. Statistical significant differences were not observed in the metabolic activity between the different groups.

the lower level of cytotoxicity. It is also necessary to compare these results between experiments, and if the results are similar, we can conclude that the results are reliable.

HT concentration influence on cytotoxicity level, within each method of sterilization

According to ISO 10993-5:2009, when performing an Indirect Contact Assay, a reduction in cell viability by more than 30% is considered a cytotoxic effect (cell viability below 70%). By analyzing Figure 6.5, we can conclude that every sample provides cell viability above 90%, meaning that none of the samples is cytotoxic.

Within the results of a given sterilization method, we performed a statistical analysis that compared each concentration group (PCL mesh, 0.03 wt%, 0.06 wt%, 0.1 wt%) with the control group (Cells). We observed no statistically significant differences between the metabolic activity of the cells ($p>0.05$).

This analysis was performed for both sterilization methods (ET+UV, UV) and for every experiment (A, B), which means that the HT concentrations group provides similar values of cell metabolic activity to the Cells group, meaning that none of these concentrations are cytotoxic.

Experiment A presents higher cell viability values than Experiment B, possibly due to different cell confluence levels.

Influence of the sterilization method on the cytotoxicity level

Horakova et al. [76] studied the impact of various sterilization and disinfection methods on an electrospun nanofibrous layer made of PCL, including EtOH soaking and UV light. For the first procedure, the authors soaked the samples in the EtOH 70% solution for 30 minutes, followed by two PBS and distilled water washes. For the disinfection via UV light, the samples were placed in a laminar flow box, and the UV light was applied for 30 minutes on each side. The authors concluded that neither of the methods influenced the fiber's morphology, molecular weight, or thermal properties. However, the EtOH soaking method results showed a higher cell viability and cell number per area, which means that this method is more effective than applying UV light.

Łopianiak et al. [80] studied different sterilization/disinfection methods of fibrous polyurethane scaffolds, including EtOH soaking and UV light. For the first method, the samples were immersed in 70% (v/v) solution at 20ºC for 20 minutes and then washed five times in sterile PBS on a plate shaker for five minutes each. The samples were irradiated for 30 minutes on each side for UV light sterilization. They concluded that neither method guaranteed high sterilization efficiency by itself.

A statistical analysis evaluated the differences between ET+UV and UV for mesh sterilization. For each concentration group (PCL mesh, 0.03 wt%, 0.06 wt%, 0.1 wt%), we compared the results from each sterilization method (ET + UV, UV) for both experiments (A, B). The observed results showed no statistically significant differences between using ET + UV or UV for the meshes' sterilization ($p>0.05$).

According to Horakova et al. [76], the ethanol soaking method provided a higher cell viability and cell number per area, so it was expected that the ET + UV method showed higher values of cell activity when compared to the UV method. On the other hand, Łopianiak et al. [80] concluded that neither method provided a highly effective sterilization. However, the methods used in both studies were different from ours. We soaked the meshes' samples in the ethanol 70% for 20 minutes instead of 30 and did not wash them with distilled water. According to Łopianiak et al. [80], the treatment duration influences the efficiency of the EtOH soaking. Besides, the materials used in both studies were not the same or could have different percentages of PCL (in the case of the study by Horakova et al. [76]). With these results, and since there are no statistically significant

differences between sterilization methods, we can conclude that both methods are adequate to sterilize these meshes correctly.

In conclusion, the HT incorporation on these meshes did not produce a cytotoxic effect on this material. These results prove that if these meshes have the right mechanical properties and behave like the native tissue, they can safely be used to treat POP without any fear of being cytotoxic to the patient, which is a promising solution for POP repair. Furthermore, we can conclude that sterilizing these meshes with ET + UV or UV methods will provide a safe and sterile biomaterial to be implanted in women.

Chapter 7

Conclusion and Future Work

7.1 Main Conclusions

We started this dissertation by introducing the health condition of Pelvic Organ Prolapse (POP) and how it impacts the lives of those suffering from it. We explored the evolution of the POP repair solutions to give insights about the pros and cons of each treatment, either invasive or not. It was shown that Polycaprolactone (PCL) biodegradable meshes may be a promising solution, as they are biodegradable, bioinert, and have a suitable degradation time.

The influence of incorporating an antistatic agent, Hostastat ® FA 38 (HT), on the fiber's diameter and PCL mechanical properties was studied by incorporating it at different concentrations (0.03, 0.06, 0.1 wt%). It was observed that the antistatic agent does have the desired effect of reducing the filament diameter. Thus, the concentration of 0.1 wt% HT provided fibers much thinner than the 0.03 and 0.06 concentrations, with a mean reduction of 65 - 66%. It was expected that the thicker the diameter, the higher the stress that the mesh could handle, which was statistically verified.

Since we are dealing with PCL/HT meshes, it was also essential to compare the obtained curves with pure PCL ones to analyze if the presence of the additive would alter the meshes' mechanical properties, namely the tensile strength and Young's Modulus. PCL/HT meshes were compared to pure PCL meshes with the same geometry and similar diameters. It was observed that, even though the PCL/HT meshes were slightly thinner than their correspondent PCL mesh, they showed a higher tensile strength and higher Young's Modulus value, with an increase of 28.41% and 55.59% for the highest HT concentration, respectively.

Other studies [8, 88, 89] also observed the influence of antistatic agents on polymers and have concluded that this incorporation modified the polymers' tensile strength, surface resistivity, and the polymer's crystallinity. These results suggest that the HT incorporation modified the PCL properties, like its crystallinity.

Lastly, the meshes' cytotoxicity was evaluated through an Indirect Contact Assay, and the metabolic activity of the cells was measured through a resazurin assay. The meshes' samples were also sterilized following two different methods: ultraviolet radiation and ethanol soaking, followed

by ultraviolet radiation. Statistical analysis proved that no HT concentration provides cytotoxicity to the meshes and that both sterilization methods are effective in sterilizing the meshes.

As a final note, we consider the HT incorporation into PCL meshes to be advantageous since it provides stable and evenly stretched filaments that result in thinner fibers. With the right HT concentration, it is possible to obtain a mesh that supports similar loads as the vaginal tissue while presenting the same level of stiffness, solving problems like stress shielding. Furthermore, it was proven that the HT incorporation with concentrations of 0.03, 0.06, and 0.1% did not have any cytotoxic effect on the biomaterial, which makes these PCL/HT meshes a promising and innovative solution that can be applied as a novel treatment for POP repair.

7.2 Future Work

A further investigation of the HT influence on the PCL mechanical properties would be of great interest to try to understand what happens to the polymer's structure that leads to a higher tensile strength and a higher stiffness. Below there is a list of tasks that could be performed in the future.

- Scanning Electron Microscopy (SEM) analysis to see detailed images of the surface morphology and microstructure of the PCL/HT and PCL meshes;
- Rheological analysis to analyze the polymer chain mobility;
- Differential Scanning Calorimetry (DSC) or a X-Ray Diffraction Analysis (XDR) to confirm if there is any modification on the polymer's crystallinity
- Study the influence of different wt% of HT on the meshes' degradation

References

[1] M. F. R. R. Vaz, "3d printing and development of 3d computational models of biodegradable meshes," M.S. thesis, Faculdade de Engenharia da Universidade do Porto, 2023.

[2] M. N. B. da Cunha, R. Rynkevic, M. E. T. da Silva, A. F. M. D. S. Brandão, J. L. Alves, and A. A. Fernandes, "Melt electrospinning writing of mesh implants for pelvic organ prolapse repair," *3D Printing and Additive Manufacturing*, vol. 9, pp. 389–398, 5 Oct. 2022, ISSN: 23297670. DOI: 10.1089/3dp.2021.0010.

[3] K. H. Choi and J. Y. Hong, "Management of pelvic organ prolapse," *Korean Journal of Urology The Korean Urological Association*, vol. 55, pp. 693–702, 2014. DOI: 10.4111/kju.2014.55.11.693&domain=pdf&date_stamp=2014-11-16. [Online]. Available: http://crossmark.crossref.org/dialog/?doi=10.411/kju.2014.55.11.693&domain=pdf&date_stamp=2014-11-16www.kjurology.orghttp://dx.doi.org/10.4111/kju.2014.55.11.693.

[4] J. Ren *et al.*, "Development of 3D Printed Biodegradable Mesh with Antimicrobial Properties for Pelvic Organ Prolapse," en, *Polymers*, vol. 14, no. 4, p. 763, Feb. 2022, Accessed 20 December 2023, ISSN: 2073-4360. DOI: 10.3390/polym14040763. [Online]. Available: https://www.mdpi.com/2073-4360/14/4/763.

[5] E. Mancuso, C. Downey, E. Doxford-Hook, M. G. Bryant, and P. Culmer, "The use of polymeric meshes for pelvic organ prolapse: Current concepts, challenges, and future perspectives," *Journal of Biomedical Materials Research - Part B Applied Biomaterials*, vol. 108, pp. 771–789, 3 Apr. 2020, ISSN: 15524981. DOI: 10.1002/jbm.b.34432.

[6] S. Loewner *et al.*, "Recent advances in melt electro writing for tissue engineering for 3d printing of microporous scaffolds for tissue engineering," *Frontiers in Bioengineering and Biotechnology*, vol. 10, Aug. 2022, ISSN: 22964185. DOI: 10.3389/fbioe.2022.896719.

[7] J. C. Kade and P. D. Dalton, "Polymers for melt electrowriting," *Advanced Healthcare Materials*, vol. 10, no. 1, p. 2 001 232, 2021. DOI: https://doi.org/10.1002/adhm.202001232. eprint: https://onlinelibrary.wiley.com/doi/pdf/10.1002/adhm.202001232. [Online]. Available: https://onlinelibrary.wiley.com/doi/abs/10.1002/adhm.202001232.

[8] W. S. Chow and W. L. Tham, "Effects of antistatic agent on the mechanical, morphological and antistatic properties of polypropylene/organo-montmorillonite nanocomposites," en, *Express Polymer Letters*, vol. 3, no. 2, pp. 116–125, 2009, Accessed 02 November 2023, ISSN: 1788618X. DOI: 10.3144/expresspolymlett.2009.15. [Online]. Available: http://www.expresspolymlett.com/letolt.php?file=EPL-0000846&mi=c.

[9] S. R. Chaudhry, A. Nahian, and K. Chaudhry, "Anatomy, Abdomen and Pelvis, Pelvis," eng, in *StatPearls*, Accessed 03 November 2023, Treasure Island (FL): StatPearls Publishing, 2023. [Online]. Available: http://www.ncbi.nlm.nih.gov/books/NBK482258/.

[10] J. M. DeSilva and K. R. Rosenberg, "Anatomy, Development, and Function of the Human Pelvis," eng, *Anatomical Record (Hoboken, N.J.: 2007)*, vol. 300, no. 4, pp. 628–632, Apr. 2017, ISSN: 1932-8494. DOI: 10.1002/ar.23561.

[11] R. F. Ferreira, "Development of a computational tool to simulate the use of synthetic meshes for pelvic organ prolapse repair," M.S. thesis, Faculdade de Engenharia da Universidade do Porto, 2020.

[12] V. Raizada and R. K. Mittal, "Pelvic Floor Anatomy and Applied Physiology," en, *Gastroenterology Clinics of North America*, vol. 37, no. 3, pp. 493–509, Sep. 2008, Accessed 03 November 2023, ISSN: 08898553. DOI: 10.1016/j.gtc.2008.06.003. [Online]. Available: https://linkinghub.elsevier.com/retrieve/pii/S0889855308000423.

[13] T. S. System, *Pelvis*, Accessed 03 November 2023. [Online]. Available: https://www.theskeletalsystem.net/pelvis.

[14] S. M. Eickmeyer, "Anatomy and Physiology of the Pelvic Floor," *Physical Medicine and Rehabilitation Clinics of North America*, Pelvic Pain, vol. 28, no. 3, pp. 455–460, Aug. 2017, Accessed 03 November 2023, ISSN: 1047-9651. DOI: 10.1016/j.pmr.2017.03.003. [Online]. Available: https://www.sciencedirect.com/science/article/pii/S10479%2065117300153.

[15] S. Todros, P. Pavan, and A. Natali, "Biomechanical properties of synthetic surgical meshes for pelvic prolapse repair," en, *Journal of the Mechanical Behavior of Biomedical Materials*, vol. 55, pp. 271–285, Mar. 2016, Accessed 01 December 2023, ISSN: 17516161. DOI: 10.1016/j.jmbbm.2015.10.024. [Online]. Available: https://linkinghub.elsevier.com/retrieve/pii/S1751616115003975.

[16] S. Rocca Rossetti, "Functional anatomy of pelvic floor," eng, *Archivio Italiano Di Urologia, Andrologia: Organo Ufficiale [di] Societa Italiana Di Ecografia Urologica E Nefrologica*, vol. 88, no. 1, pp. 28–37, Mar. 2016, ISSN: 1124-3562. DOI: 10.4081/aiua.2016.1.28.

[17] A. Braga and M. Serati, "New Advances in Female Pelvic Floor Dysfunction Management," eng, *Medicina (Kaunas, Lithuania)*, vol. 59, no. 6, p. 1010, May 2023, ISSN: 1648-9144. DOI: 10.3390/medicina59061010.

[18] Z. Ghanbari *et al.*, "Quality of Life Following Pelvic Organ Prolapse Treatments in Women: A Systematic Review and Meta-Analysis," *Journal of Clinical Medicine*, vol. 11, no. 23, p. 7166, Dec. 2022, Accessed 03 November 2023, ISSN: 2077-0383. DOI: 10.3390/jcm11237166. [Online]. Available: https://www.ncbi.nlm.nih.gov/pmc/articles/PMC9738239/.

[19] C. Maher, B. Feiner, K. Baessler, C. Christmann-Schmid, N. Haya, and J. Marjoribanks, "Transvaginal mesh or grafts compared with native tissue repair for vaginal prolapse," *The Cochrane Database of Systematic Reviews*, vol. 2016, no. 2, p. CD012079, Feb. 2016, Accessed 03 November 2023, ISSN: 1469-493X. DOI: 10.1002/14651858.CD012079. [Online]. Available: https://www.ncbi.nlm.nih.gov/pmc/articles/PMC6489145/.

[20] R. Gong and Z. Xia, "Collagen changes in pelvic support tissues in women with pelvic organ prolapse," en, *European Journal of Obstetrics & Gynecology and Reproductive Biology*, vol. 234, pp. 185–189, Mar. 2019, Accessed 01 May 2024, ISSN: 03012115. DOI: 10.1016/j.ejogrb.2019.01.012. [Online]. Available: https://linkinghub.elsevier.com/retrieve/pii/S0301211519300399.

[21] C. Clinic, *Pelvic organ prolapse*, Accessed 28 November 2023. [Online]. Available: https://my.clevelandclinic.org/health/diseases/24046-pelvic-organ-prolapse.

[22] A. Bartuzi, K. Futyma, B. Kulik-Rechberger, and T. Rechberger, "Self-perceived quality of life after pelvic organ prolapse reconstructive mesh surgery: Prospective study," en, *European Journal of Obstetrics & Gynecology and Reproductive Biology*, vol. 169, no. 1, pp. 108–112, Jul. 2013, Accessed 03 November 2023, ISSN: 03012115. DOI: 10.1016/j.ejogrb.2013.03.018. [Online]. Available: https://linkinghub.elsevier.com/retrieve/pii/S0301211513001632.

[23] T. Belayneh, A. Gebeyehu, M. Adefris, G. Rortveit, J. L. Gjerde, and T. A. Ayele, "Pelvic organ prolapse surgery and health-related quality of life: A follow-up study," *BMC Women's Health*, vol. 21, p. 4, Jan. 2021, Accessed 03 November 2023, ISSN: 1472-6874. DOI: 10.1186/s12905-020-01146-8. [Online]. Available: https://www.ncbi.nlm.nih.gov/pmc/articles/PMC7778798/.

[24] T. Cadenbach-Blome, M. Grebe, M. Mengel, F. Pauli, A. Greser, and C. Fünfgeld, "Significant Improvement in Quality of Life, Positive Effect on Sexuality, Lasting Reconstructive Result and Low Rate of Complications Following Cystocele Correction Using a Lightweight, Large-Pore, Titanised Polypropylene Mesh," en, *Geburtshilfe und Frauenheilkunde*, vol. 79, no. 09, pp. 959–968, Sep. 2019, Publisher: Georg Thieme Verlag KG, ISSN: 0016-5751,

1438-8804. DOI: 10.1055/a-0984-6614. [Online]. Available: http://www.thieme-connect.de/DOI/DOI?10.1055/a-0984-6614.

[25] E. P. Ubertazzi, H. F. Soderini, A. J. Saavedra Sanchez, C. Fonseca Guzman, and L. I. Paván, "Long-term outcomes of transvaginal mesh (TVM) In patients with pelvic organ prolapse: A 5-year follow-up," en, *European Journal of Obstetrics & Gynecology and Reproductive Biology*, vol. 225, pp. 90–94, Jun. 2018, Accessed 03 November 2023, ISSN: 03012115. DOI: 10.1016/j.ejogrb.2018.03.060. [Online]. Available: https://linkinghub.elsevier.com/retrieve/pii/S0301211518301581.

[26] A. Gauthier, P. Ferry, P. Bertherat, R. De Tayrac, and H. Fernandez, "Transvaginal treatment of anterior and apical genital prolapse using Restorelle® direct fix™: An observational study of medium-term complications and outcomes," en, *Journal of Gynecology Obstetrics and Human Reproduction*, vol. 49, no. 2, p. 101 674, Feb. 2020, Accessed 01 December 2023, ISSN: 24687847. DOI: 10.1016/j.jogoh.2019.101674. [Online]. Available: https://linkinghub.elsevier.com/retrieve/pii/S246878471930707X.

[27] R. Rynkevic, M. Silva, P. Martins, T. Mascarenhas, J. Alves, and A. Fernandes, "Characterisation of polycaprolactone scaffolds made by melt electrospinning writing for pelvic organ prolapse correction - a pilot study," en, *Materials Today Communications*, vol. 32, p. 104 101, Aug. 2022, Accessed 01 December 2023, ISSN: 23524928. DOI: 10.1016/j.mtcomm.2022.104101. [Online]. Available: https://linkinghub.elsevier.com/retrieve/pii/S2352492822009539.

[28] Coloplast, *Coloplast*, Accessed 05 January 2024. [Online]. Available: https://www.coloplast.pt/.

[29] M. Russo Serafini *et al.*, "3D-Printed Medical-Grade Polycaprolactone (mPCL) Scaffold for the Surgical Treatment of Vaginal Prolapse and Abdominal Hernias," en, *Bioengineering*, vol. 10, no. 11, p. 1242, Oct. 2023, Accessed 06 January 2024, ISSN: 2306-5354. DOI: 10.3390/bioengineering10111242. [Online]. Available: https://www.mdpi.com/2306-5354/10/11/1242.

[30] U.S. Food and Drug Administration, *Fda takes action to protect women's health, orders manufacturers of surgical mesh intended for transvaginal repair of pelvic organ prolapse to stop selling all devices*, Accessed 05 January 2024. [Online]. Available: https://www.fda.gov/news-events/press-announcements/fda-takes-action-protect-womens-health-orders-manufacturers-surgical-mesh-intended-transvaginal.

[31] K. M. Knight, P. A. Moalli, and S. D. Abramowitch, "Preventing Mesh Pore Collapse by Designing Mesh Pores With Auxetic Geometries: A Comprehensive Evaluation Via Computational Modeling," en, *Journal of Biomechanical Engineering*, vol. 140, no. 5, p. 051 005, May 2018, Accessed 08 April 2024, ISSN: 0148-0731, 1528-8951. DOI: 10.1115/1.4039058. [Online]. Available: https://asmedigitalcollection.asm

e.org/biomechanical/article/doi/10.1115/1.4039058/422054/Preventing-Mesh-Pore-Collapse-by-Designing-Mesh.

[32] L.-M. Zhu, "Mesh implants: An overview of crucial mesh parameters," en, *World Journal of Gastrointestinal Surgery*, vol. 7, no. 10, p. 226, 2015, Accessed 20 June 2024, ISSN: 1948-9366. DOI: 10.4240/wjgs.v7.i10.226. [Online]. Available: http://www.wjgnet.com/1948-9366/full/v7/i10/226.htm.

[33] S. Sterk, "Development of new surgical mesh geometries with different mechanical properties using the design freedom of 3d printing," M.S. thesis, Faculdade de Engenharia da Universidade do Porto / Frankfurt University of Applied Sciences, 2023.

[34] C. K. Chua, C. H. Wong, and W. Y. Yeong, "Chapter One - Introduction to 3D Printing or Additive Manufacturing," in *Standards, Quality Control, and Measurement Sciences in 3D Printing and Additive Manufacturing*, C. K. Chua, C. H. Wong, and W. Y. Yeong, Eds., Accessed 19 May 2024, Academic Press, Jan. 2017, pp. 1–29, ISBN: 978-0-12-813489-4. DOI: 10.1016/B978-0-12-813489-4.00001-5. [Online]. Available: https://www.sciencedirect.com/science/article/pii/B9780128134894000015.

[35] F. Afghah, C. Dikyol, M. Altunbek, and B. Koc, "Biomimicry in Bio-Manufacturing: Developments in Melt Electrospinning Writing Technology Towards Hybrid Biomanufacturing," en, *Applied Sciences*, vol. 9, no. 17, p. 3540, Aug. 2019, Accessed 17 October 2023, ISSN: 2076-3417. DOI: 10.3390/app9173540. [Online]. Available: https://www.mdpi.com/2076-3417/9/17/3540.

[36] M. Pérez, D. Carou, E. M. Rubio, and R. Teti, "Current advances in additive manufacturing," *Procedia CIRP*, 13th CIRP Conference on Intelligent Computation in Manufacturing Engineering, 17-19 July 2019, Gulf of Naples, Italy, vol. 88, pp. 439–444, Jan. 2020, Accessed 22 June 2024, ISSN: 2212-8271. DOI: 10.1016/j.procir.2020.05.076. [Online]. Available: https://www.sciencedirect.com/science/article/pii/S2212827120303978.

[37] T. D. Ngo, A. Kashani, G. Imbalzano, K. T. Q. Nguyen, and D. Hui, "Additive manufacturing (3D printing): A review of materials, methods, applications and challenges," *Composites Part B: Engineering*, vol. 143, pp. 172–196, Jun. 2018, Accessed 22 June 2024, ISSN: 1359-8368. DOI: 10.1016/j.compositesb.2018.02.012. [Online]. Available: https://www.sciencedirect.com/science/article/pii/S1359836817342944.

[38] A. Youssef, S. J. Hollister, and P. D. Dalton, "Additive manufacturing of polymer melts for implantable medical devices and scaffolds," en, *Biofabrication*, vol. 9, no. 1, p. 012 002, Feb. 2017, Accessed 01 November 2023, ISSN: 1758-5090. DOI: 10.1088/1758-5090/aa5766. [Online]. Available: https://iopscience.iop.org/article/10.1088/1758-5090/aa5766.

[39] N. Arifin, I. Sudin, N. H. A. Ngadiman, and M. S. A. Ishak, "A Comprehensive Review of Biopolymer Fabrication in Additive Manufacturing Processing for 3D-Tissue-Engineering Scaffolds," en, *Polymers*, vol. 14, no. 10, p. 2119, May 2022, Accessed 18 December 2023, ISSN: 2073-4360. DOI: 10.3390/polym14102119. [Online]. Available: https://www.mdpi.com/2073-4360/14/10/2119.

[40] P. D. Dalton, "Melt electrowriting with additive manufacturing principles," *Current Opinion in Biomedical Engineering*, vol. 2, pp. 49–57, 2017, Additive Manufacturing, ISSN: 2468-4511. DOI: https://doi.org/10.1016/j.cobme.2017.05.007. [Online]. Available: https://www.sciencedirect.com/science/article/pii/S2468451117300156.

[41] Y. Liu, K. Li, M. M. Mohideen, and S. Ramakrishna, "Development of melt electrospinning," en, in *Melt Electrospinning*, Accessed 01 November 2023, Elsevier, 2019, pp. 1–5, ISBN: 978-0-12-816220-0. DOI: 10.1016/B978-0-12-816220-0.00001-4. [Online]. Available: https://linkinghub.elsevier.com/retrieve/pii/B9780128162200000014.

[42] K. D. Patel, A. R. Padalhin, R. A. G. Franco, F. Verisqa, H. W. Kim, and L. Nguyen, "Basic concepts and fundamental insights into electrospinning," en, in *Biomedical Applications of Electrospinning and Electrospraying*, Accessed 01 November 2023, Elsevier, 2021, pp. 3–43, ISBN: 978-0-12-822476-2. DOI: 10.1016/B978-0-12-822476-2.00010-8. [Online]. Available: https://linkinghub.elsevier.com/retrieve/pii/B9780128224762000108.

[43] R. Jose Varghese, E. hadji Mamour Sakho, S. Parani, S. Thomas, O. S. Oluwafemi, and J. Wu, "Chapter 3 - introduction to nanomaterials: Synthesis and applications," in *Nanomaterials for Solar Cell Applications*, S. Thomas, E. H. M. Sakho, N. Kalarikkal, S. O. Oluwafemi, and J. Wu, Eds., Elsevier, 2019, pp. 75–95, ISBN: 978-0-12-813337-8. DOI: https://doi.org/10.1016/B978-0-12-813337-8.00003-5. [Online]. Available: https://www.sciencedirect.com/science/article/pii/B9780128133378000035.

[44] K. Morikawa, M. Green, and M. Naraghi, "A Novel Approach for Melt Electrospinning of Polymer Fibers," en, *Procedia Manufacturing*, vol. 26, pp. 205–208, 2018, Accessed 01 November 2023, ISSN: 23519789. DOI: 10.1016/j.promfg.2018.07.028. [Online]. Available: https://linkinghub.elsevier.com/retrieve/pii/S235197891830698X.

[45] N. Sheoran, B. Boland, S. Thornton, J. R. Bochinski, and L. I. Clarke, "Increasing ionic conductivity within thermoplastics via commercial additives results in a dramatic decrease in fiber diameter from melt electrospinning," *Soft Matter*, vol. 17, pp. 9264–9279, 41 2021. DOI: 10.1039/D1SM01101D. [Online]. Available: http://dx.doi.org/10.1039/D1SM01101D.

[46] M. Precision, *Electrospinning (formation of ultra-fine polymer fibers)*, Accessed 02 November 2023. [Online]. Available: https://www.matsusada.com/application/ps/electrospinning/.

[47] J. Xue, T. Wu, Y. Dai, and Y. Xia, "Electrospinning and Electrospun Nanofibers: Methods, Materials, and Applications," en, *Chemical Reviews*, vol. 119, no. 8, pp. 5298–5415, Apr. 2019, Accessed 30 May 2024, ISSN: 0009-2665, 1520-6890. DOI: 10.1021/acs.chemrev.8b00593. [Online]. Available: https://pubs.acs.org/doi/10.1021/acs.chemrev.8b00593.

[48] T. Matsuura and M. M. A. Shirazi, "Principles of electrospinning and nanofiber membranes," en, in *Electrospun and Nanofibrous Membranes*, Accessed 01 November 2023, Elsevier, 2023, pp. 3–25, ISBN: 978-0-12-823032-9. DOI: 10.1016/B978-0-12-823032-9.00016-7. [Online]. Available: https://linkinghub.elsevier.com/retrieve/pii/B9780128230329000167.

[49] G. Hochleitner *et al.*, "Additive manufacturing of scaffolds with sub-micron filaments via melt electrospinning writing," *Biofabrication*, vol. 7, no. 3, p. 035 002, Jun. 2015. DOI: 10.1088/1758-5090/7/3/035002. [Online]. Available: https://dx.doi.org/10.1088/1758-5090/7/3/035002.

[50] R. P. A. Hartman, D. J. Brunner, D. M. A. Camelot, J. C. M. Marijnissen, and B. Scarlett, "ELECTROHYDRODYNAMIC ATOMIZATION IN THE CONE–JET MODE PHYSICAL MODELING OF THE LIQUID CONE AND JET," *Journal of Aerosol Science*, vol. 30, no. 7, pp. 823–849, 1999, ISSN: 0021-8502. DOI: https://doi.org/10.1016/S0021-8502(99)00033-6. [Online]. Available: https://www.sciencedirect.com/science/article/pii/S0021850299000336.

[51] T. D. Brown, P. D. Dalton, and D. W. Hutmacher, "Melt electrospinning today: An opportune time for an emerging polymer process," *Progress in Polymer Science*, vol. 56, pp. 116–166, 2016, ISSN: 0079-6700. DOI: https://doi.org/10.1016/j.progpolymsci.2016.01.001. [Online]. Available: https://www.sciencedirect.com/science/article/pii/S0079670016000022.

[52] Y. Xie, Q. Fang, H. Zhao, Y. Li, Z. Lin, and J. Chen, "Effects of Six Processing Parameters on the Size of PCL Fibers Prepared by Melt Electrospinning Writing," *Micromachines*, vol. 14, no. 7, p. 1437, Jul. 2023, Accessed 02 November 2023, ISSN: 2072-666X. DOI: 10.3390/mi14071437. [Online]. Available: https://www.ncbi.nlm.nih.gov/pmc/articles/PMC10385759/.

[53] F.-L. He *et al.*, "Investigation of the effects of melt electrospinning parameters on the direct-writing fiber size using orthogonal design," *Journal of Physics D: Applied Physics*, vol. 50, no. 42, p. 425 601, Sep. 2017. DOI: 10.1088/1361-6463/aa8901. [Online]. Available: https://dx.doi.org/10.1088/1361-6463/aa8901.

[54] Y. Jin *et al.*, "Fabrication of heterogeneous scaffolds using melt electrospinning writing: Design and optimization," en, *Materials & Design*, vol. 185, p. 108 274, Jan. 2020, Accessed 13 December 2023, ISSN: 02641275. DOI: 10.1016/j.matdes.2019.108274. [Online]. Available: https://linkinghub.elsevier.com/retrieve/pii/S0264127519307129.

[55] M. L. Muerza-Cascante, D. Haylock, D. W. Hutmacher, and P. D. Dalton, "Melt electrospinning and its technologization in tissue engineering," *National Library of Medicine*, vol. 21, no. 2, Dec. 2014. DOI: 10.1089/ten.TEB.2014.0347. [Online]. Available: https://doi/10.1089/ten.teb.2014.0347.

[56] E. H. Backes *et al.*, "Polycaprolactone usage in additive manufacturing strategies for tissue engineering applications: A review," en, *Journal of Biomedical Materials Research Part B: Applied Biomaterials*, vol. 110, no. 6, pp. 1479–1503, Jun. 2022, Accessed 18 December 2023, ISSN: 1552-4973, 1552-4981. DOI: 10.1002/jbm.b.34997. [Online]. Available: https://onlinelibrary.wiley.com/doi/10.1002/jbm.b.34997.

[57] G. V. da Silva Santos Nunes, "Bioengineered novel contraction-blocking biomaterials for skin tissue engineering," M.S. thesis, Faculdade de Engenharia da Universidade do Porto / Instituto de Ciências Biomédicas Abel Salazar, 2023.

[58] C. Maier and T. Calafut, "Polypropylene," in *Polypropylene*, ser. Plastics Design Library, C. Maier and T. Calafut, Eds., Norwich, NY: William Andrew Publishing, 1998, ch. 3, pp. 27–47, ISBN: 978-1-884207-58-7. DOI: https://doi.org/10.1016/B978-188420758-7.50008-4. [Online]. Available: https://www.sciencedirect.com/science/article/pii/B9781884207587500084.

[59] R. Höfer, "Processing and Performance Additives for Plastics," en, in *Polymer Science: A Comprehensive Reference*, Accessed 17 October 2023, Elsevier, 2012, pp. 369–381, ISBN: 978-0-08-087862-1. DOI: 10.1016/B978-0-444-53349-4.00272-7. [Online]. Available: https://linkinghub.elsevier.com/retrieve/pii/B9780444533494002727.

[60] J. Pionteck, "INTRODUCTION," en, in *Handbook of Antistatics*, Accessed 17 October 2023, Elsevier, 2016, pp. 1–15, ISBN: 978-1-895198-95-9. DOI: 10.1016/B978-1-895198-95-9.50003-0. [Online]. Available: https://linkinghub.elsevier.com/retrieve/pii/B9781895198959500030.

[61] Clariant, *Clariant*, Accessed 03 April 2024. [Online]. Available: https://www.clariant.com/pt/Corporate.

[62] K. Miller, J. Hsu, and L. Soslowsky, "Materials in tendon and ligament repair," in *Comprehensive Biomaterials*, P. Ducheyne, Ed., Oxford: Elsevier, 2011, pp. 257–279, ISBN: 978-0-08-055294-1. DOI: https://doi.org/10.1016/B978-0-08-055294-1.00218-X. [Online]. Available: https://www.sciencedirect.com/science/article/pii/B978008055294100218X.

[63] G. Manivasagam, A. Reddy, D. Sen, S. Nayak, M. T. Mathew, and A. Rajamanikam, "Dentistry: Restorative and regenerative approaches," in *Encyclopedia of Biomedical Engineering*, R. Narayan, Ed., Oxford: Elsevier, 2019, pp. 332–347, ISBN: 978-0-12-805144-3. DOI: https://doi.org/10.1016/B978-0-12-801238-3.11017-7. [Online]. Available: https://www.sciencedirect.com/science/article/pii/B9780128012383110177.

[64] Piyasin, Yensano, and Pinitsoontorn, "Size-Controllable Melt-Electrospun Polycaprolactone (PCL) Fibers with a Sodium Chloride Additive," en, *Polymers*, vol. 11, no. 11, p. 1768, Oct. 2019, Accessed 02 November 2023, ISSN: 2073-4360. DOI: 10.3390/polym11111768. [Online]. Available: https://www.mdpi.com/2073-4360/11/11/1768.

[65] M. Shahverdi, S. Seifi, A. Akbari, K. Mohammadi, A. Shamloo, and M. R. Movahhedy, "Melt electrowriting of PLA, PCL, and composite PLA/PCL scaffolds for tissue engineering application," en, *Scientific Reports*, vol. 12, no. 1, p. 19 935, Nov. 2022, Accessed 01 June 2024, ISSN: 2045-2322. DOI: 10.1038/s41598-022-24275-6. [Online]. Available: https://www.nature.com/articles/s41598-022-24275-6.

[66] C. K. Arakawa and C. A. DeForest, "Chapter 19 - polymer design and development," in *Biology and Engineering of Stem Cell Niches*, A. Vishwakarma and J. M. Karp, Eds., Boston: Academic Press, 2017, pp. 295–314, ISBN: 978-0-12-802734-9. DOI: https://doi.org/10.1016/B978-0-12-802734-9.00019-6. [Online]. Available: https://www.sciencedirect.com/science/article/pii/B9780128027349000196.

[67] J. Ren *et al.*, "Development of 3d printed biodegradable mesh with antimicrobial properties for pelvic organ prolapse," *Polymers*, vol. 14, 4 Feb. 2022, ISSN: 20734360. DOI: 10.3390/polym14040763.

[68] E. Malikmammadov, T. E. Tanir, A. Kiziltay, V. Hasirci, and N. Hasirci, "Pcl and pcl-based materials in biomedical applications," *Journal of Biomaterials Science, Polymer Edition*, vol. 29, pp. 863–893, 7-9 Jun. 2018, ISSN: 15685624. DOI: 10.1080/09205063.2017.1394711.

[69] 3D4Makers, *3d4makers filament engineers*, Accessed 03 April 2024. [Online]. Available: https://www.3d4makers.com/.

[70] C. P. what matters, *Corbion*, Accessed 03 April 2024. [Online]. Available: https://www.corbion.com/.

[71] A. V. Rane, K. Kanny, V. Abitha, and S. Thomas, "Methods for Synthesis of Nanoparticles and Fabrication of Nanocomposites," en, in *Synthesis of Inorganic Nanomaterials*, Accessed 10 January 2024, Elsevier, 2018, pp. 121–139, ISBN: 978-0-08-101975-7. DOI: 10.1016/B978-0-08-101975-7.00005-1. [Online]. Available: https://linkinghub.elsevier.com/retrieve/pii/B9780081019757000051.

[72] Fractory, *Stress-strain curve*, Accessed 17 May 2023. [Online]. Available: https://fractory.com/stress-strain-curve/.

[73] S. L. Edwards, J. A. Werkmeister, A. Rosamilia, J. A. Ramshaw, J. F. White, and C. E. Gargett, "Characterisation of clinical and newly fabricated meshes for pelvic organ prolapse repair," en, *Journal of the Mechanical Behavior of Biomedical Materials*, vol. 23, pp. 53–61, Jul. 2013, Accessed 20 December 2023, ISSN: 17516161. DOI: 10.1016/j.jmbbm.2013.04.002. [Online]. Available: https://linkinghub.elsevier.com/retrieve/pii/S1751616113001239.

[74] D. Yalcin, "Tensile testing concepts & definitions," *Materials Testing System Manufacturer*, 2021.

[75] M. Omidi *et al.*, "Characterization of biomaterials," en, in *Biomaterials for Oral and Dental Tissue Engineering*, Accessed 25 May 2024, Elsevier, 2017, pp. 97–115, ISBN: 978-0-08-100961-1. DOI: 10.1016/B978-0-08-100961-1.00007-4. [Online]. Available: https://linkinghub.elsevier.com/retrieve/pii/B9780081009611000074.

[76] J. Horakova *et al.*, "Impact of Various Sterilization and Disinfection Techniques on Electrospun Polycaprolactone," *ACS Omega*, vol. 5, no. 15, pp. 8885–8892, Apr. 2020, Publisher: American Chemical Society. DOI: 10.1021/acsomega.0c00503. [Online]. Available: https://doi.org/10.1021/acsomega.0c00503.

[77] L. Preem *et al.*, "Effects and efficacy of different sterilization and disinfection methods on electrospun drug delivery systems," *International Journal of Pharmaceutics*, vol. 567, p. 118 450, Aug. 2019, Accessed 20 June 2024, ISSN: 0378-5173. DOI: 10.1016/j.ijpharm.2019.118450. [Online]. Available: https://www.sciencedirect.com/science/article/pii/S0378517319304843.

[78] T. A. M. Valente, D. M. Silva, P. S. Gomes, M. H. Fernandes, J. D. Santos, and V. Sencadas, "Effect of Sterilization Methods on Electrospun Poly(lactic acid) (PLA) Fiber Alignment for Biomedical Applications," *ACS Applied Materials & Interfaces*, vol. 8, no. 5, pp. 3241–3249, Feb. 2016, Publisher: American Chemical Society, ISSN: 1944-8244. DOI: 10.1021/acsami.5b10869. [Online]. Available: https://doi.org/10.1021/acsami.5b10869.

[79] C. Gualandi *et al.*, "Ethanol disinfection affects physical properties and cell response of electrospun poly(l-lactic acid) scaffolds," *European Polymer Journal*, vol. 48, no. 12, pp. 2008–2018, Dec. 2012, Accessed 20 June 2024, ISSN: 0014-3057. DOI: 10.1016/j.eurpolymj.2012.09.016. [Online]. Available: https://www.sciencedirect.com/science/article/pii/S0014305712003114.

[80] I. Łopianiak and B. A. Butruk-Raszeja, "Evaluation of Sterilization/Disinfection Methods of Fibrous Polyurethane Scaffolds Designed for Tissue Engineering Applications," en, *International Journal of Molecular Sciences*, vol. 21, no. 21, p. 8092, Jan. 2020, Number: 21 Publisher: Multidisciplinary Digital Publishing Institute, ISSN: 1422-0067. DOI: 10.3390/ijms21218092. [Online]. Available: https://www.mdpi.com/1422-0067/21/21/8092.

[81] J. Petiti, L. Revel, and C. Divieto, "Standard Operating Procedure to Optimize Resazurin-Based Viability Assays," en, *Biosensors*, vol. 14, no. 4, p. 156, Apr. 2024, Number: 4 Publisher: Multidisciplinary Digital Publishing Institute, ISSN: 2079-6374. DOI: 10.3390/bios14040156. [Online]. Available: https://www.mdpi.com/2079-6374/14/4/156.

[82] Alchemer, *How to choose between parametric & nonparametric tests*, Accessed 21 June 2024. [Online]. Available: https://www.alchemer.com/resources/blog/how-to-choose-between-parametric-nonparametric-tests/.

[83] H. to Mechatronics, *G-code explained*, Accessed 10 April 2023. [Online]. Available: https://howtomechatronics.com/tutorials/g-code-explained-list-of-most-important-g-code-commands/.

[84] FullControl, *Fullcontrol gcode designer*, Accessed 11 March 2024. [Online]. Available: https://fullcontrolgcode.com/.

[85] N. Viewer, *Nc viewer v1.1.3*, Accessed 11 March 2024. [Online]. Available: https://ncviewer.com/.

[86] Mecmesin, *Multitest-dv motorised force test*, Accessed 16 May 2023. [Online]. Available: https://www.mecmesin.com/motorised-force-test-stands/motorised-force-tester.

[87] M. I. A. Pinto, "Melt electrowriting prototype optimization for medical-grade polycaprolactone mesh printing," M.S. thesis, Faculty of Engineering of the University of Porto, 2022.

[88] Y. Zhao, Y. Liu, H. Zhao, and Z. Chen, "The synthesis of a novel polymer-type antistatic agent and its effect on the properties of polypropylene," en, *Journal of Applied Polymer Science*, vol. 141, no. 27, e55589, 2024, Accessed 20 June 2024, ISSN: 1097-4628. DOI: 10.1002/app.55589. [Online]. Available: https://onlinelibrary.wiley.com/doi/abs/10.1002/app.55589.

[89] N. Sun *et al.*, "Fabrication of Permanent Antistatic PMMA Copolymer for Enhanced Antistatic and Mechanical Properties," *ACS Applied Polymer Materials*, vol. 5, no. 7, pp. 5537–5543, Jul. 2023, Publisher: American Chemical Society. DOI: 10.1021/acsapm.3c00833. [Online]. Available: https://doi.org/10.1021/acsapm.3c00833.